

# juliet: a versatile modelling tool for transiting and non-transiting exoplanetary systems

Néstor Espinoza<sup>1,2★†‡</sup>, Diana Kossakowski<sup>1</sup>, Rafael Brahm<sup>3,4,5</sup>

<sup>1</sup> *Max-Planck-Institut für Astronomie, Königstuhl 17, 69117 Heidelberg, Germany.*

<sup>2</sup> *Space Telescope Science Institute, 3700 San Martin Drive, Baltimore, MD 21218, USA.*

<sup>3</sup> *Center of Astro-Engineering UC, Pontificia Universidad Católica de Chile, Av. Vicuña Mackenna 4860, 7820436 Macul, Santiago, Chile.*

<sup>4</sup> *Instituto de Astrofísica, Facultad de Física, Pontificia Universidad Católica de Chile, Av. Vicuña Mackenna 4860, 782-0436 Macul, Santiago, Chile.*

<sup>5</sup> *Millennium Institute of Astrophysics, Av. Vicuña Mackenna 4860, 782-0436 Macul, Santiago, Chile.*

Accepted XXX. Received YYY; in original form ZZZ

## ABSTRACT

Here we present *juliet*, a versatile tool for the analysis of transits, radial-velocities, or both. *juliet* is built over many available tools for the modelling of transits, radial-velocities and stochastic processes (here modelled as Gaussian Processes; GPs) in order to deliver a tool/wrapper which can be used for the analysis of transit photometry and radial-velocity measurements from multiple instruments at the same time, using nested sampling algorithms which allows it to not only perform a thorough sampling of the parameter space, but also to perform model comparison via bayesian evidences. In addition, *juliet* allows to fit transiting and non-transiting multi-planetary systems, and to fit GPs which might share hyperparameters between the photometry and radial-velocities simultaneously (e.g., stellar rotation periods), which might be useful for disentangling stellar activity in radial-velocity measurements. Nested Sampling, Importance Nested Sampling and Dynamic Nested Sampling is performed with publicly available codes which in turn give *juliet* multi-threading options, allowing it to scale the computing time of complicated multi-dimensional problems. We make *juliet* publicly available via GitHub.

**Key words:** methods: data analysis – methods: statistical – techniques: photometric – techniques: radial velocities – planets and satellites: fundamental parameters – planets and satellites: individual: K2-140b, K2-32b, c, d

## 1 INTRODUCTION

The pioneering efforts from both ground-based radial-velocity (see, e.g., [Queloz et al. 2000](#); [Tinney et al. 2001](#); [Pepe et al. 2004](#); [Bouchy et al. 2009](#); [Arriagada 2011](#); [Butler et al. 2017](#); [Reiners et al. 2018](#)) and transit (see, e.g. [Pollacco et al. 2006](#); [Nutzman & Charbonneau 2008](#); [Wheatley et al. 2013](#); [Burdanov et al. 2017](#); [Pepper et al. 2018](#); [Bakos 2018](#)) surveys, along with ambitious space-based transit searches ([Borucki et al. 2010](#); [Ricker et al. 2015](#)), has transformed and nurtured the known field today of extrasolar planets. These efforts have not only increased the number of known planets

outside of the solar system from just a couple to thousands<sup>1</sup> in about a decade, but have also unveiled the diversity of worlds orbiting stars other than our Sun.

The data with which the vast majority of the above mentioned discoveries has been made is, in general, extensive, and has given rise to various analysis tools at different steps of the process. These tools range from detection and validation algorithms that help to reject possible false-positive scenarios and/or disentangle the planetary signals from other possible signals causing the observed data (see, e.g., [Hartman et al. 2009](#); [Morton 2012](#); [Díaz et al. 2014](#); [Morton 2015](#); [Faria et al. 2018](#)) to analysis tools used to retrieve the physical and orbital parameters of the discovered exoplanets from observed lightcurves (see, e.g., [Gazak et al.](#)

★ E-mail: nespinoza@stsci.edu (NE)

† Bernoulli Fellow

‡ IAU-Gruber Fellow

<sup>1</sup> Over 3000 at the time of writing according to <http://www.exoplanets.org/> ([Wright et al. 2011](#)).

2012; Parviainen 2015), radial-velocities (see, e.g., Meschiari et al. 2009; Wright & Howard 2009; Baluev 2013; Iglesias-Marzoa et al. 2015; Malavolta et al. 2016; Fulton et al. 2018; Faria et al. 2018) or both (see, e.g., Bakos et al. 2010; Hartman et al. 2012; Espinoza et al. 2016; Baluev 2018; Barragán et al. 2019; Günther & Daylan 2019; Foreman-Mackey et al. 2019), some of which even include the modelling of the stellar properties jointly with the modelling of the photometry and radial-velocities (Eastman et al. 2013; Eastman 2017; Eastman et al. 2019; Hartman et al. 2018).

As can be seen from the above, a plethora of tools are available in the literature to perform analyses of exoplanetary signals in order to constrain the physical parameters of an orbit given either photometry, radial-velocities or both. In terms of planet discovery and characterization, tools that can fit both photometry and radial velocities coming from different instruments simultaneously will be extremely important, as missions like the *Transiting Exoplanet Survey Satellite* (TESS; Ricker et al. 2015) are already starting to provide thousands of new interesting exoplanets orbiting bright stars which will receive extensive follow-up, especially from radial-velocity facilities, that needs to be analyzed in detail in order to reveal the physical parameters of the transiting object.

In this work we introduce an open source library developed to perform exactly the kind of analysis discussed above, which has many differences and improvements over other available tools that perform similar tasks (e.g., Eastman et al. 2013; Eastman 2017; Eastman et al. 2019; Baluev 2018; Barragán et al. 2019). First, this new library allows for the fitting of any number of transiting and non-transiting systems, allowing a simultaneous fit of the available data coming from either photometry, radial-velocities or both. It also allows Gaussian Processes (Rasmussen & Williams 2006) to be fitted both to the photometry (with a different gaussian process to each photometric instrument) and the radial velocities, allowing even for common hyperparameters of these Gaussian Processes to be shared between both datasets — useful, e.g., in settings in which rotational modulation information (such as a characteristic stellar rotation period) is present both in the photometry and in the radial-velocities. In addition, our procedures are efficient at exploring the whole parameter space thanks to nested sampling algorithms used in the parameter exploration procedure which, due to their nature, allow us to also estimate the probability of different models given the data through bayesian evidences (e.g., eccentric orbits, additional planets in the system, different model for systematic trends, etc.). This library, *juliet*, is publicly available at GitHub<sup>2</sup> and is written in Python.

Before detailing the procedures used by *juliet* to model the data and showcase the types of analysis it can do, we would like to first motivate how it differentiates itself from existing codes that perform similar tasks and, thus, why such a library is needed. To date and to our knowledge, the seven open-source tools that can perform both photometric and radial-velocity analysis in order to constrain the physical and orbital parameters of a transiting exoplanet are EXOFAST (Eastman et al. 2013; Eastman 2017; Eastman

et al. 2019), *exonailer* (Espinoza et al. 2016), *PlanetPack* (Baluev 2018), *pyaneti* (Barragán et al. 2019), *PyORBIT* (Malavolta et al. 2016, 2018), *allesfitter* (Günther & Daylan 2019) and *exoplanet* (Foreman-Mackey et al. 2019). EXOFAST is one of the most versatile of the tools described: it indeed allows to fit photometry and radial-velocities from different instruments, and even allows to perform the modelling of the stellar properties jointly with the available photometry and radial-velocity measurements. However, one of its weaknesses is its inability to account for different noise processes in both the photometry and radial-velocities such as Gaussian Processes (Rasmussen & Williams 2006), which might impact directly on, e.g., the type of radial-velocity signals that it can handle and in the type of photometry that is able to simultaneously detrend, which in some cases might not be well modelled by the simple linear models in the parameters that it can currently handle. *exonailer* (Espinoza et al. 2016), although allowing to fit radial-velocities and photometry from different instruments as well, it is not as versatile as EXOFAST. It does allow to detrend photometry in its most recent versions via Gaussian Processes, but because it uses *emcee* (Foreman-Mackey et al. 2013) to perform the parameter exploration, is very sensitive to the initial parameters, often making this simultaneous detrending procedure of the photometry unfeasible to be performed jointly with the transit and radial-velocity parameter optimization. In addition, *exonailer* is currently able to fit only one planet at the time, and does not allow to model Gaussian Processes in the radial-velocities either. *PyORBIT* (Malavolta et al. 2016, 2018) does allow to fit transits and radial-velocities simultaneously, allowing to fit multiple-planets simultaneously. It does also incorporate Gaussian Processes but it also uses *emcee* for the parameter exploration, which makes it prompt to the same problems of initial values as *exonailer*. *PlanetPack* in its most recent version (Baluev 2018) incorporates the modelling of Gaussian Processes for the radial-velocity modelling, and allows to fit for a variety of effects including simultaneous transit fitting along with the radial-velocity optimization. This code, however, only allows to account for systematic trends in the photometry via polynomials, and does not allow to fit multiplanetary systems in the photometry. The recently introduced *pyaneti* (Barragán et al. 2019), although allowing to fit multiple planets in both the radial-velocities and transits, it does not allow to handle data obtained from multiple photometric instruments, and does not support the use of Gaussian Processes either in the photometry nor in the radial-velocities. Finally, *allesfitter* (Günther & Daylan 2019) and *exoplanet* (Foreman-Mackey et al. 2019) are both very similar to *juliet* — these are projects that were, in fact, developed at about the same time than this one. While *allesfitter* at the time of writing is able to fit for a wide range of phenomena *including* transit and radial-velocities, we believe *juliet* is much more user-friendly given its thorough documentation<sup>3</sup> and importability into *python* scripts. While these latter benefits are shared with *exoplanet*, *juliet* is an excellent alternative if what one is looking for is to perform model comparison via bayesian evidences (see below) *and* posterior sampling — currently, only the latter is allowed by *exoplanet*.

<sup>2</sup> <https://github.com/nespinoza/juliet>

<sup>3</sup> <https://juliet.readthedocs.io/en/latest/>

There is one additional weakness shared by almost all the open source joint fitting tools just described above (with the only exception being `allesfitter`): none of them provide tools to perform formal model comparison between different models used to fit the data. Although `PlanetPack` and `EXOFAST` do provide (frequentist) statistics on the fits performed to the data, it is not straightforward to use those to compare different models, as all frequentist statistical measures assume an underlying null hypothesis which does not take into account either prior information nor the reality that there are more models than the one being tested. This is very important for complicated tasks such as calculating the evidence for additional planets in either the transits and/or the radial-velocities (especially in the case in which extra, non-planetary signals such as stellar activity might make this procedure even more difficult), or even for more simple but routine tasks such as finding evidence for an eccentric orbit (or even disentangling between significant eccentricity or additional planets; see e.g., Kürster et al. 2015). Although this question has been explored in the literature for the detection of planets in radial-velocities (see, e.g. the excellent discussion on this topic by Nelson et al. 2018, and references therein) and even open source tools have been developed to aid in quantifying this evidence (Faria et al. 2018), no general open source tool is available for this that allows to incorporate transits and radial-velocities coming from data from different instruments. From our discussion, we believe there is thus a strong need for a tool that can incorporate both linear and Gaussian Process regression in both transits and radial-velocities, that can take into account multiple-planet systems, and that can, on top of that, provide a quantitative measure of the evidence of different models so that they can be compared and be either selected or combined in a formal manner. This is the main motivation behind `juliet`.

This work, which introduces our `juliet` library, is organized as follows. Section 2 presents how the data modelling is treated within `juliet`. In Section 3 we present some tests of the code on real data, with which we show some its capabilities. Section 4 presents a discussion and in 5 we present our conclusions and future work.

## 2 DATA MODELLING WITHIN JULIET

In this section, we introduce the probabilistic models `juliet` assumes when performing photometric and/or radial-velocity fits to data. For both of those types of datasets, `juliet` considers a common model in which each datapoint  $y(t_{i,l})$  at time  $t_{i,l}$ , with  $i$  being an index that identifies each instrument and  $l$  being an index identifying a datapoint in a given instrument (i.e.,  $l \in [0, 1, \dots, N_i]$ , where  $N_i$  is the total number of datapoints in instrument  $i$ ) is given by a probabilistic model of the form:

$$y(t_{i,l}) \sim \mathcal{M}_i(t_{i,l}) + \text{LM}_i(t_{i,l}) + \epsilon_i(t_{i,l}). \quad (1)$$

Here,  $\mathcal{M}_i(t_{i,l})$  denotes the particular photometric (described in Section 2.1) or radial-velocity (described in Section 2.2) model for instrument  $i$ , which depends on the physical planetary parameters of the system being modelled (e.g., the planet-to-star radius ratio for transits or the semi-amplitude for radial-velocities) as well as instrumental parameters (e.g., the limb-darkening parameters for transit

models, or the systemic velocities of each instrument for radial-velocities).  $\text{LM}_i$  is a linear model for instrument  $i$  of the form

$$\text{LM}_i(t_{i,l}) = \sum_{n=0}^{p_i} x_{n,i}(t_{i,l}) \theta_{n,i}^{\text{LM}}, \quad (2)$$

where the  $x_{n,i}(t_{i,l})$  are the  $p_i + 1$  linear regressors at time  $t_{i,l}$  for instrument  $i$ , and  $\theta_{n,i}^{\text{LM}}$  are the coefficients of those regressors (e.g.,  $x_{n,i}(t_{i,l}) = t_{i,l}^n$  would model a polynomial trend for instrument  $i$ ). Finally,  $\epsilon_i(t_{i,l})$  is a zero-mean noise term, which `juliet` can model in various forms including Gaussian Processes (GPs; Rasmussen & Williams 2006, see Section 2.3 for details on the kernels that `juliet` can handle). As will be detailed in Section 2.3, this term can be either an individual term for each instrument, or be common to all instruments, where the dependance with each instrument in this latter case is only through a jitter term unique to each instrument,  $\sigma_{w,i}$ .

Given thus the vector of the *physical parameters of the planets* that define the photometric or radial-velocity models (i.e., the vector containing all the physical elements that define each model),  $\vec{\theta}_P$ , `juliet` can handle two types of possible models for either the photometry or the radial-velocities. The first is an “instrument-by-instrument” model in which the log-likelihood of each instrument is assumed to be different (i.e., each instrument has its own individual noise model with possible common hyperparameters with other instruments). In this case, the full log-likelihood considering all the instruments is easily separable as a sum of log-likelihoods for each instrument (because they are independent from each other). If we consider the vector that defines each instrumental model  $\vec{\theta}_i$  (which includes, e.g., the coefficients  $\theta_{n,i}^{\text{LM}}$  of the linear model for each instrument and the hyperparameters of the chosen noise model for instrument  $i$ ) and the vector  $\vec{y}_i = (y(t_{i,0}), y(t_{i,1}), \dots, y(t_{i,N_i}))^T$  which has the probabilistic model for all the datapoints in instrument  $i$ , then the total log-likelihood of the model considering the data of all instruments,  $\mathcal{D}_I$ , for the whole photometric or radial-velocity model has a common form, given by

$$\ln p(\mathcal{D}_I | \vec{\theta}_P, \vec{\theta}_0, \vec{\theta}_1, \dots) = \sum_{i=0} \ln p(\vec{y}_i | \vec{\theta}_P, \vec{\theta}_i), \quad (3)$$

where in general we assume the likelihood for each instrument follows the likelihood of a  $N_i$ -dimensional multivariate gaussian, i.e.,

$$\ln p(\vec{y}_i | \vec{\theta}_P, \vec{\theta}_i) = -\frac{1}{2} \left[ N_i \ln 2\pi + \ln |\Sigma_i| + \vec{r}_i^T \Sigma_i^{-1} \vec{r}_i \right],$$

where each element of vector  $\vec{r}_i$ ,  $r_{i,l}$ , is given by

$$r_{i,l} = y_i(t_{i,l}) - \mathcal{M}_i(t_{i,l}) - \text{LM}_i(t_{i,l}).$$

The second type of model `juliet` is able to handle is a so-called “global” model, in which the noise model for either the whole photometric or radial-velocity dataset is *common* to all instruments. In this case,  $\epsilon_i(t_{i,l}) \equiv \epsilon(t_{i,l}) + \tilde{\epsilon}_i(t_{i,l})$ , where  $\tilde{\epsilon}_i(t_{i,l}) \sim N(0, \sigma_{w,i}^2 + \sigma_{t_{i,l}}^2)$ , and where  $N(\mu, \sigma^2)$  denotes a normal distribution with mean  $\mu$  and variance  $\sigma^2$ . Here,  $\sigma_{t_{i,l}}^2$  are the formal uncertainties for datapoint  $y(t_{i,l})$ , and  $\sigma_{w,i}^2$  is a jitter term that can be defined or fitted for instrument  $i$ .

Here, the whole dataset  $\mathcal{D}_I$  is modelled together without specific noise models on each instrument (apart for

the white-noise part individual to each instrument,  $\bar{\epsilon}_i(t_{i,l})$ ). Considering the stacked data vector  $\vec{y}$  containing all the data  $y(t_{i,l})$  for all instruments, and the stacked parameter vector containing all the physical and instrumental parameters,  $\vec{\theta}$ , the total log-likelihood is in this case of the form

$$\ln p(\vec{y}|\vec{\theta}) = -\frac{1}{2} \left[ N_I \ln 2\pi + \ln |\Sigma_I| + \vec{r}^T \Sigma_I^{-1} \vec{r} \right], \quad (4)$$

where  $N_I = \sum N_i$ . Here, each element of the residual vector  $\vec{r}$ ,  $r(t_{i,l})$  is given by

$$r(t_{i,l}) = y(t_{i,l}) - \mathcal{M}_i(t_{i,l}) - \text{LM}_i(t_{i,l}).$$

In this case, thus, the elements of the covariance matrix  $\Sigma_I$  are given by

$$\Sigma_I(t_{i,l}, t_{j,m}) = k(x_{i,l}, x_{j,m}) + (\sigma_{w,i}^2 + \sigma_{t_{i,l}}^2) \delta_{t_{i,l}, t_{j,m}}$$

with  $\delta_{t_{i,l}, t_{j,m}}$  a Kronecker's delta, and  $k(\cdot)$  being either zero for a pure white-noise model, or equal to any of the kernels defined in Section 2.3.

It is important to distinguish the physical significance of the “instrument-by-instrument” model given in equation (3) and the “global” model given in equation (4). Because the former assumes a different noise model for each instrument, this model assumes each instrument provides a distinct realization of a noise process. That is, even if two instruments share *all* the hyperparameters of the noise model, those two instruments are modelled as if their observed noise processes were generated by different realizations of the same process. The “global” model, however, assumes that not only all instruments share the hyperparameters of the selected noise model: it assumes *all come from exactly the same realization of the process*. This latter model, thus, is typically very useful for observations of physical processes (e.g., rotational modulation in either photometry or radial-velocities) with the same instrument over different seasons, and/or similar instruments, whereas the former model is typically useful for observations of instruments with different bandpasses and/or different underlying noise processes.

## 2.1 Photometric modelling

The model within `juliet` assumed for the photometry for each instrument,  $\mathcal{M}_i(t_{i,l})$ , is of the form

$$\mathcal{M}_i(t_{i,l}) = [\mathcal{T}_i(t_{i,l})D_i + (1 - D_i)] \left( \frac{1}{1 + D_i M_i} \right). \quad (5)$$

Here,  $\mathcal{T}_i(t_{i,l})$  is the full transit model including any number of  $N_p^T$  planets in the system for instrument  $i$ ,  $D_i$  is a dilution factor for the given instrument and  $M_i$  is a mean offset out-of-transit flux. The parameters that define the photometric model (described in detail below) are given in Table 1.

The motivation behind the model defined in (5) is that precise photometric instruments like *TESS* will provide photometry that will be contaminated by the flux of nearby sources due to its large pixel size (e.g., 21" for *TESS*, [Ricker et al. 2015](#)), which will in turn contaminate the “true” transit parameters due to this dilution of the transit shape by nearby light sources to the target star. In addition, the model is also motivated by the work of [Kipping & Tinetti \(2010\)](#) which predicts so-called “self-dilution” of a planet might happen due to light from the exoplanet’s night-side diluting the transit signature. To understand the process of this dilution,

**Table 1.** List of parameters that define the model  $\mathcal{M}_i(t_{i,l})$  for the photometry for instrument  $i$ . Note that the same planetary parameters have to be given to every planet in the system.

Parameter name	Units	Description
Planetary parameters		
$P$	days	Orbital period.
$t_0$	days	Time of transit-center.
$p$	—	Planet-to-star radius ratio <sup>1</sup> .
$b$	—	Impact parameter <sup>1</sup> .
$a/R_*$	—	Scaled semi-major axis <sup>2</sup> .
$e$	—	Eccentricity of the orbit <sup>3</sup> .
$\omega$	deg	Argument of periastron <sup>3</sup> .
Instrumental parameters <sup>4</sup>		
$D_i$	—	Dilution factor.
$M_i$	relative flux	Relative flux offset.
$q_{1,i}$	—	Limb-darkening parameter <sup>5</sup> .
$q_{2,i}$	—	Limb-darkening parameter <sup>5</sup> .

<sup>1</sup> Instead of fitting directly for  $(p, b)$ , `juliet` allows to fit for  $(r_1, r_2)$ , which samples the whole range of physically plausible values for  $p$  and  $b$  (see [Espinoza 2018](#), for details).

<sup>2</sup> Instead of the scaled semi-major axis, the stellar density  $\rho_*$  (in units of  $\text{kg/m}^3$ ) can be fitted. If this is the case, for multiple-planet fits only one value is needed to constrain  $a_k/R_*$  of all the  $k$  planets (see text).

<sup>3</sup> Instead of fitting for  $(e, \omega)$  directly, `juliet` allows to fit for the first and second Laplace parameters  $\mathcal{E}_1 = e \sin \omega$  and  $\mathcal{E}_2 = e \cos \omega$  or the parameters  $S_1 = \sqrt{e} \sin \omega$  and  $S_2 = \sqrt{e} \cos \omega$ . This latter parametrization is recommended.

<sup>4</sup> In addition, the coefficients for the linear models,  $\theta_{n,i}^{\text{LM}}$ , can optionally be defined if linear regressors are fed to `juliet`.

<sup>5</sup> Note these are *not* the limb-darkening coefficients, except for the linear law, where  $q_2 = 0$  and  $q_1 = u$ , the linear limb-darkening coefficients. The mapping of these parameters to the limb-darkening coefficients is described in [Kipping \(2013\)](#) and [Espinoza & Jordán \(2016\)](#) (see text).

how this impacts on the transit model  $\mathcal{T}(t)$  and what the parameters in equation (5) mean, let  $F_T$  be the out-of-transit flux of the target star in a given passband and let  $\sum_n F_n$  be the total flux of any  $n$  other sources in the photometric aperture used to obtain the observed flux of the target as a function of time,  $F_O(t)$  (note that among the  $n$  sources in this formalism, a subset might actually be the flux of the planets transiting the target star themselves, which would give rise to the “self-dilution” effect discussed in [Kipping & Tinetti \(2010\)](#)). This latter flux will thus be given by

$$F_O(t) = \mathcal{T}(t)F_T + \sum_n F_n.$$

In this formalism,  $\mathcal{T}(t)$  will be one for out-of-transit times  $t$  and less than one at in-transit times, implying that the *physical* out-of-transit flux will be simply  $F_T + \sum_n F_n$ . Typically, if available, one would estimate this out-of-transit flux (via, e.g., the mean, median, etc. of the out-of-transit measurements) and compute relative fluxes by simply dividing this estimate to the observed flux  $F_O(t)$ . However, in reality there is no guarantee there will actually be out of transit flux in order to estimate it from the data (from, e.g., follow-up transit lightcurves), and thus one performs an estimate of the out-of-transit flux on the data that might deviate from this physical picture. Let us assume the *estimated* out-of-transit flux is of the form  $F_T + \sum_n F_n + E$ , where  $E$  is a real



constant representing the offset flux from the real out-of-transit flux (note this flux could be negative; e.g., in the case in which this estimate comes from the median of the observations of a transit with no or very little out-of-transit measurements, or where it is not clear where the out-of-transit flux actually is located in time). With this, the relative flux  $\hat{F}_O(t) = F_O(t)/(F_T + \sum_n F_n + E)$  will thus be given (after some rearrangements) by

$$\hat{F}_O(t) = [\mathcal{T}(t)D + (1 - D)] \left( \frac{1}{1 + D(E/F_T)} \right), \quad (6)$$

where

$$D = \frac{1}{1 + \sum_n F_n/F_T}.$$

Comparing equation (6) with equation (5), one can see that if the photometric datapoints  $y(t_{i,l})$  are relative fluxes, in the absence of a linear model one can physically interpret the expected values of  $D_i$  and  $M_i$  in equation (5) directly with the terms in (6). On one hand, because  $\sum_n F_n/F_T > 0$ , this implies that the dilution factor  $0 \leq D_i \leq 1$  and thus that *the smaller  $D_i$  is, the largest the dilution by instrument  $i$  is*. This parametrization for the dilution factor  $D_i$  is thus very useful because it gives a strict support to this parameter. As for  $M_i$ , this factor controls and fits for the relative (and arbitrary) offset (with respect to the target flux) that was applied to generate the observed data  $y_i^P(t_l)$ . This offset (relative, with respect to the target) flux can vary in sign and value, but is always around zero for data whose relative fluxes have been estimated with plenty of out-of-transit flux; in the worst case scenarios, this factor can be of the same order as the transit depth. In general,  $D_i M_i > -1$ . It is interesting to note that given this physical interpretation for  $D_i$  and  $M_i$ , one might put priors on these parameters given known apertures and diluting sources (e.g., for the case of TESS, using the TESS input catalog; Stassun et al. 2018). However, it is important to note that the diluting sources could also be of instrumental (e.g., miscalculated background flux) and/or astrophysical (e.g., as is the case for “self”-dilutions discussed above) origin, and as such care must be taken when imposing strong priors on those parameters. Similarly, care must be taken if one chooses to put too wide of a prior (e.g., uniform between 0 and 1) on this parameter as it could lead to, e.g., a large transit depth with a very small dilution factor in low signal-to-noise transits. These cases should, thus, be always inspected and interpreted in order to decide the best model for a given dataset.

Within **juliet**, the transit model  $\mathcal{T}_i(t_{i,l})$ , is generated by using **batman** (Kreidberg 2015), which has many flexible options useful for transit modelling including the supersampling of the lightcurve model in cases of long-cadence integrations (for details, see Kipping 2010), a mode that is, thanks to **batman**, also implemented within **juliet**. In our library, the full transit model  $\mathcal{T}_i(t_l)$  is actually obtained by subtracting 1 to the transit model of each of the  $N_p^T$  planets, which gives us the percentage of light each planet is obscuring; then, all the contributions are added up, which gives us the total percentage of light occulted by all the planets. We add 1 to this result in order to have a normalized total transit lightcurve. This allows **juliet** to efficiently fit multi-planetary transiting systems with the caveat that although our code is able to model multiple planets obscuring the

stellar surface simultaneously, *it is not able to model planet-planet transits* (see, e.g., Luger et al. 2017, and references therein). The transit parameters that are allowed to vary for each transiting planet  $k \in [1, \dots, N_p^T]$  (where for simplicity, we drop the subscript  $k$  to identify its parameters in what follows unless otherwise stated) are the planet-to-star radius ratio,  $p = R_p/R_s$ , the semi-major axis in stellar units,  $a/R_*$ , the impact parameter of the orbit,  $b = (a/R_*)\cos i_p$ , where  $i_p$  is the inclination of the planetary orbit with respect to the plane of the sky, the period of the orbit  $P$ , the time of transit center  $t_0$ , the argument of periastron passage  $\omega$  and the eccentricity of the orbit,  $e$ . In practice, **juliet** allows to parametrize either  $p$  and  $b$  directly, or using the efficient sampling scheme detailed in Espinoza (2018) in which two parameters  $r_1$  and  $r_2$  defined between 0 and 1 are sampled and which explore all the physically meaningful ranges for  $p$  and  $b$  in the  $(b, p)$  plane, which ensures the condition  $b < 1 + p$  is always satisfied without the need to perform rejection sampling (i.e., reject samples for which  $b \geq 1 + p$ ). In addition, and for reasons that will be detailed in Section 2.4, within **juliet** we also allow to fit for a common stellar density for all the transiting exoplanets in the system,  $\rho_*$ , instead of individual values of  $a/R_*$  for each transiting exoplanet in the system. The eccentricity and argument of periastron passage can either be parametrized within **juliet** (1) directly, (2) using the first and second Laplace parameters  $\mathcal{E}_1 = e \sin \omega$  and  $\mathcal{E}_2 = e \cos \omega$ , in which case the eccentricity and argument of periastron are defined as  $e = \sqrt{\mathcal{E}_1^2 + \mathcal{E}_2^2}$  and  $\omega = \text{atan2}(\mathcal{E}_1, \mathcal{E}_2)$  (which, as noted by Ford 2006, puts a pathological prior of  $p(e) = e$  on the eccentricity) or (3) via the transformations  $\mathcal{S}_1 = \sqrt{e} \sin \omega$  and  $\mathcal{S}_2 = \sqrt{e} \cos \omega$ , in which case  $e = \mathcal{S}_1^2 + \mathcal{S}_2^2$  and  $\omega = \text{atan2}(\mathcal{S}_1, \mathcal{S}_2)$ ; for an excellent discussion on the advantages and disadvantages of those parametrizations, see Eastman et al. (2013). It is important to note here that in practice in order to generate a transit model, **batman** needs the inclination and not the impact parameter of a given planet in order to generate its transit model. To transform the impact parameter in order to obtain the inclination of the orbit in the general case of eccentric orbits, **juliet** calculates the inclination as (see, e.g., Winn 2010):

$$i_p = \arccos \left[ \frac{b}{a/R_*} \left( \frac{1 + e \sin \omega}{1 - e^2} \right) \right],$$

which is, of course, valid as long the term inside the arccos is  $\leq 1$ . For limb-darkening, **juliet** does not use a direct parametrization of the limb-darkening coefficients as the philosophy within **juliet** is to, whenever possible, *fit for* the limb-darkening coefficients in the analysis, as the procedure of fixing limb-darkening coefficients to values obtained from stellar models is known to give rise to biases in the derived transit parameters for precise transit lightcurves such as the ones obtained by the *Kepler* mission and the ones currently being obtained by *TESS* (Espinoza & Jordán 2015, 2016). Moreover, given the importance of using different limb-darkening laws for different systems/instruments, **juliet** allows to fit any one or two-parameter law available via **batman** which includes the linear, quadratic, square-root and logarithmic laws — the exponential limb-darkening law is not included in this list as it might give rise to unphysical results (Espinoza & Jordán 2016). In practice, for the two-parameter laws, **juliet** uses the parametrization pro-

posed by [Kipping \(2013\)](#), where two parameters  $q_{i,1}$  and  $q_{i,2}$  defined between 0 and 1 are sampled (one pair for each photometric instrument  $i$  used in the analysis) in order to produce, for a given limb-darkening law, only physically plausible limb-darkening coefficients for the selected laws, which imply that the intensities are everywhere positive and produce decreasing gradients towards the limb of the star. For all the two-parameter laws but the logarithmic **juliet** uses the transformations derived in [Kipping \(2013\)](#) to go from the  $(q_{i,1}, q_{i,2})$  plane to the limb-darkening coefficients  $(u_{i,1}, u_{i,2})$  plane; for the logarithmic law, **juliet** uses the transformations derived in [Espinoza & Jordán \(2016\)](#). For the linear law, **juliet** uses one parameter  $q_i \equiv u_i$  which defines the intensity profile of the star. It is important to mention here that while the parameters of a given planet in the transit model (i.e.,  $p$ ,  $a/R_*$ ,  $b$ ,  $P$ ,  $t_0$ ,  $\omega$ ,  $e$ ) are all the same along instruments, **juliet** uses one set of limb-darkening coefficients which is unique to each instrument and *common among different planets observed with the same instrument*. This might seem intuitive as all the planets in a given system are transiting the same star. However, retrieved limb-darkening coefficients are also known to depend on the geometry of the system even *for the same star* ([Howarth 2011](#)). In practice, however, we believe the errors on the retrieved limb-darkening coefficients are not precise enough to see this latter differences on multiplanetary systems and, as such, decide within **juliet** to have one common set of limb-darkening coefficients per instrument. **juliet** also allows for each instrument to have its own limb-darkening law, as the bias/variance tradeoff on the retrieval of transit parameters from transit lightcurves when fitting for the limb-darkening coefficients is known to scale differently depending on the number of datapoints, geometry of the system and response function (see, e.g., [Espinoza & Jordán 2016](#)).

## 2.2 Radial-velocity modelling

The corresponding model  $\mathcal{M}_i(t_{i,l})$  used within **juliet** to model the radial-velocities for each instrument is given by

$$\mathcal{M}_i(t_{i,l}) = \mathcal{K}(t_{i,l}) + \mu_i + Q \left( t'_{i,l} \right)^2 + A t'_{i,l} + B.$$

Here,  $\mathcal{K}(t_{i,l})$  is a full Keplerian signal including any number of  $N_p^{\text{RV}}$  planets in the system,  $\mu_i$  is an instrument-dependant systemic velocity and  $Q$ ,  $A$  and  $B$  define optional quadratic and linear terms along with the corresponding intercept, respectively, of a long-term trend present on the data (coming from, e.g., additional long-period companions/activity whose period is unconstrained by the current data). This latter trend — common to all instruments — in turn, depends on  $t'_{i,l} = t_{i,l} - t_a$ , where  $t_a$  is an arbitrary user-defined time (default within **juliet** is  $t_a = 2458460$ ). Table 2 lists all the parameters (described in detail below) needed to define the radial-velocity model.

To compute a model for the Keplerian signal,  $\mathcal{K}(t_{i,l})$ , **juliet** uses **radvel** ([Fulton et al. 2018](#)), which easily implements any number of radial-velocity planetary signals in its modelling, and thus allows us to consider multiplanetary signals (as a sum of Keplerians, i.e., neglecting dynamical interactions *between* exoplanets; see [Laughlin 2003](#)). The parameters that **juliet** uses to define the model for the Keplerian of planet  $k \in [1, \dots, N_p^{\text{RV}}]$  are the semi-amplitude of

**Table 2.** List of parameters that define the model  $\mathcal{M}_i(t_{i,l})$  for the radial-velocities (RVs) for instrument  $i$ . Note that the same planetary parameters have to be given to every planet in the system.

Parameter name	Units	Description
Planetary parameters		
$P$	days	Orbital period.
$t_0$	days	Time of transit-center.
$K$	m/s or km/s	RV semi-amplitude.
$e$	—	Eccentricity of the orbit <sup>1</sup> .
$\omega$	deg	Argument of periastron <sup>1</sup> .
Instrumental parameters <sup>2,3</sup>		
$\mu_i$	m/s or km/s	Systemic RV.

<sup>1</sup> Instead of fitting for  $(e, \omega)$  directly, **juliet** allows to fit for the first and second Laplace parameters  $\mathcal{E}_1 = e \sin \omega$  and  $\mathcal{E}_2 = e \cos \omega$  or the parameters  $\mathcal{S}_1 = \sqrt{e} \sin \omega$  and  $\mathcal{S}_2 = \sqrt{e} \cos \omega$ . This latter parametrization is recommended.

<sup>2</sup> In addition, the coefficients for the linear models,  $\theta_{n,i}^{\text{LM}}$ , can optionally be defined if linear regressors are fed to **juliet**.

<sup>3</sup> Additionally, one can fit quadratic (through the parameter  $Q$ , with units of (m/s)/day<sup>2</sup> or (km/s)/day<sup>2</sup>) and linear trends (through the parameter  $A$ , with units of (m/s)/day or (km/s)/day<sup>2</sup>), which in turn can involve an intercept term ( $B$ , with units m/s or km/s).

the variation,  $K_k$ , the period of the orbit,  $P_k$ , the time of transit center,  $t_{0,k}$ , the argument of periastron passage,  $\omega_k$  and the eccentricity of the orbit,  $e_k$  (with these latter two parameters being able to be parametrized as defined in the previous sub-section for the photometry). Note that all the parameters but  $K_k$  are common with the transit model for each planet present in the system. Also note that **juliet** allows either  $N_p^{\text{RV}} = N_p^{\text{T}}$  (i.e., both planets transit *and* show radial velocity signatures),  $N_p^{\text{RV}} > N_p^{\text{T}}$  (i.e., only a subset of the planets in the system transit) and  $N_p^{\text{RV}} < N_p^{\text{T}}$  (i.e., only a subset of the transiting planets show radial-velocity signatures).

## 2.3 Noise models supported within juliet

As described at the beginning of this Section, currently **juliet** allows to adopt different forms for the noise model  $\epsilon_i(t_{i,l})$  defined in equation (1), in order to allow flexibility in the modelling structure. The simplest form of this noise model is that of a white-noise model. In this case, this term is assumed to be of the form

$$\epsilon_i(t_{i,l}) \sim N(0, \sigma_{w,i}^2 + \sigma_{t_{i,l}}^2).$$

Here,  $\sigma_{w,i}$  is a jitter term added in quadrature to each of the errorbars of each datapoint,  $\sigma_{t_{i,l}}$ , which can be left as a free parameter or fixed in the fit. This very simple form in turn implies that the covariance matrix  $\Sigma_i$ , needed to evaluate equation (3), is simply a diagonal matrix with terms  $\sigma_{w,i}^2 + \sigma_{t_{i,l}}^2$  in the diagonal, which implies this is the fastest noise model **juliet** can currently handle, as it requires no matrix inversions.

The simple white-noise model, however, is inadequate in most cases. Correlated noise-structures, quasi-periodic signals and/or systematic trends which can only be fit by

large-degree polynomials are common to find in general. Because of these possibilities, within *juliet* one can model the noise term as a GP in order to have a non-parametric approach to use in those different situations. If assumed as a multi-dimensional GP, then *juliet* assumes  $\epsilon_i(t_{i,l}) \sim \mathcal{GP}(0, \Sigma_i(\mathbf{X}_i))$ , where  $\mathcal{GP}(\vec{0}, \Sigma_i(\mathbf{X}_i))$  is a multi-dimensional GP with  $\mathbf{X}_i$  being a  $D_i \times N_i$  matrix containing the  $D_i$  external parameters that define the GP kernel for instrument  $i$ , which in turn defines the  $N_i \times N_i$  covariance matrix of the process  $\Sigma_i$ . The elements of the covariance matrix (for which we'll drop the  $i$  subscript for simplicity in what follows, along with the one for the  $\mathbf{X}_i$  matrix), are in turn defined to be of the form

$$\Sigma_{l,m} = k_l(\vec{x}_l, \vec{x}_m) + (\sigma_{w,i}^2 + \sigma_{t_{i,l}}^2) \delta_{l,m}, \quad (7)$$

where the terms  $\sigma_{w,i}$  and  $\sigma_{t_{i,l}}$  have already been defined,  $\delta_{l,m}$  is a Kronecker's delta and  $k_l(\vec{x}_l, \vec{x}_m)$  is the kernel of the GP for instrument  $l$ , with  $\vec{x}_l$  and  $\vec{x}_m$  being column vectors of columns  $l$  and  $m$  of the  $\mathbf{X}$  matrix. Currently, *juliet* supports the flexible squared-exponential kernel in its  $D_i$ -dimensional form given by

$$k_i(\vec{x}_l, \vec{x}_m) = \sigma_{\mathcal{GP}_i}^2 \exp \left( - \sum_{d=1}^{D_i} \alpha_d (x_{d,l} - x_{d,m})^2 \right).$$

Here,  $x_{d,l}$  and  $x_{d,m}$  are elements  $(d,l)$  and  $(d,m)$  of the  $\mathbf{X}$  matrix; the  $\alpha_d$  with  $d \in [0, \dots, D_i]$  and  $\sigma_{\mathcal{GP}_i}$  are the hyperparameters of the GP. The  $\alpha_d$ , on one hand, are inverse (squared) length-scale parameters that could be interpreted as the importance of each external parameter in our kernel and  $\sigma_{\mathcal{GP}_i}$  can be interpreted as the parameter defining the total amplitude of the process. This form of the squared-exponential kernel has been motivated by the work of Gibson et al. (2012); Gibson (2014), and its success on the modelling of systematic trends present in precise transit lightcurves of both ground and space-based observatories. To evaluate the log-likelihood implied by this GP, within *juliet* we use the *george*<sup>4</sup> package (Ambikasaran et al. 2014).

Another of the kernels currently supported by *juliet* given a vector of inputs  $\vec{x}$ , is either an exponential GP of the form

$$k_i(x_l, x_m) = \sigma_{\mathcal{GP}_i}^2 \exp(-\tau/T_i),$$

where  $\tau = |x_l - x_m|$ , and the kernel is defined by its hyperparameters  $\sigma_{\mathcal{GP}_i}$  and  $T_i$ , or with an approximate Matern kernel of the form

$$k_i(x_l, x_m) = \sigma_{\mathcal{GP}_i}^2 \left[ (1 + 1/\epsilon) e^{-(1-\epsilon)s_i} + (1 - 1/\epsilon) e^{-(1+\epsilon)s_i} \right],$$

with  $s_i = \sqrt{3}\tau/\rho_i$ , with hyperparameters  $\sigma_{\mathcal{GP}_i}$  and  $\rho_i$ , and with  $\epsilon$  set to 0.01 (note that as  $\epsilon \rightarrow 0$ , this latter kernel converges to a Matern 3/2 kernel; this form and this interpretation was interpreted by Foreman-Mackey et al. 2017). We also consider as a possible kernel the one resulting from their multiplication (and which thus only has a common amplitude  $\sigma_{\mathcal{GP}_i}^2$ ). The latter kernels are introduced and used by *juliet* as they are computed using *celerite*<sup>5</sup> (Foreman-Mackey et al. 2017), which provides a very fast means to fit

for long term trends in datasets with large number of datapoints where classical algorithms for GP regression would be too slow. This speed improvement, however, comes at a cost: this algorithm can only be applied if the input values are one-dimensional. Also, in practice, the  $\vec{x}$  vector has to be sorted in ascending order (e.g., time is a very good input variable).

Finally, *juliet* also supports quasi-periodic GP kernels, useful for modelling rotational modulation signals in photometric measurements or activity signals in radial-velocities. The implied covariance matrix follows the same structure as the one defined in equation (7), but for a kernel *juliet* either uses a quasi-periodic exp-sine-squared kernel multiplied by a squared exponential kernel (a model introduced in Haywood et al. 2014, for the analysis of photometric and RV data), which can be used with any (one) external parameter (e.g., time), the very flexible quasi-periodic kernel introduced in Foreman-Mackey et al. (2017) or the more general stochastically-driven damped simple harmonic oscillator (SHO, also introduced in Foreman-Mackey et al. 2017, for GP regression). The former is of the form

$$k_i(x_l, x_m) = \sigma_{\mathcal{GP}_i}^2 \exp \left( -\alpha_i \tau^2 - \Gamma_i \sin^2 \left[ \frac{\pi \tau}{P_{\text{rot},i}} \right] \right), \quad (8)$$

and has hyperparameters  $\sigma_{\mathcal{GP}_i}$ ,  $\alpha_i$ ,  $\Gamma_i$  and  $P_{\text{rot},i}$ , with the latter defining the period of the quasi-periodic oscillations<sup>6</sup>. We again use the *george*<sup>7</sup> package within *juliet* to compute the implied log-likelihood this process implies. On the other hand, the flexible quasi-periodic kernel introduced in Foreman-Mackey et al. (2017) is of the form

$$k_i(x_l, x_m) = \frac{B_i}{2 + C_i} e^{-\tau/L_i} \left[ \cos \left( \frac{2\pi \tau}{P_{\text{rot},i}} \right) + (1 + C_i) \right], \quad (9)$$

where  $B_i$ ,  $C_i$ ,  $L_i$  and  $P_{\text{rot},i}$  are the hyperparameters of the model, with the latter corresponding to the period of the quasi-periodic oscillations defined by this kernel. The advantage of the latter model is that it is faster to perform the computations required for the matrix inversions of the implied covariance matrix as the computations within *juliet* for it are generated with *celerite*. Finally, the SHO kernel implemented within *juliet* thanks to its *celerite* implementation (Foreman-Mackey et al. 2017) is of the form

$$k_i(x_l, x_m) = S_0 \omega_0 Q e^{-\frac{\omega_0 \tau}{2Q}} \begin{cases} f_1(\omega_0, \tau, Q) & \text{for } 0 < Q < 1/2, \\ f_2(\omega_0, \tau) & \text{for } Q = 1/2, \\ f_3(\omega_0, \tau, Q) & \text{for } Q > 1/2, \end{cases}$$

where

$$\begin{aligned} f_1(\omega_0, \tau, Q) &= \cosh(\eta \omega_0 \tau) + \frac{1}{2\eta Q} \sinh(\eta \omega_0 \tau), \\ f_2(\omega_0, \tau) &= 2(1 + \omega_0 \tau), \\ f_3(\omega_0, \tau, Q) &= \cos(\eta \omega_0 \tau) + \frac{1}{2\eta Q} \sin(\eta \omega_0 \tau), \end{aligned}$$

with  $\eta = |1 - 1/(4Q^2)|^{1/2}$ . This kernel is very useful for the modelling of active regions in a stellar surface as was noted by Foreman-Mackey et al. (2017) and also used by Ribas

<sup>4</sup> <https://github.com/dfm/george>

<sup>5</sup> <https://github.com/dfm/celerite>

<sup>6</sup> In the notation of Haywood et al. (2014),  $\sigma_{\mathcal{GP}_i} = \eta_1$ ,  $\alpha = 1/2\eta_2^2$ ,  $P_{\text{rot}} = \eta_3$  and  $\Gamma = 2/\eta_4^2$ . Note here the interpretation of  $\alpha$  as an inverse squared time-scale.

<sup>7</sup> <https://github.com/dfm/george>

et al. (2018) in the context of modelling stellar activity in radial-velocities.

## 2.4 Stellar density modelling

As it is widely known, the scaled semi-major axis and the orbital period, parameters obtainable from transiting exoplanet lightcurves, allows us to get the stellar density of the star hosting the planets which, via Kepler’s third law, is given by  $\hat{\rho}_* = [(3\pi)/(GP_k^2)](a_k/R_*)^3$ , where  $G = 6.67408 \times 10^{-11} \text{ m}^3 \text{ kg}^{-1} \text{ s}^{-2}$  is the gravitational constant, a fact already noted by Sozzetti et al. (2007) to constrain the stellar parameters using transit lightcurves. However, thanks to the precise measurements provided by Gaia Data Release 2 (Gaia Collaboration et al. 2018), we are currently in an era where stellar parameters allow us to do the opposite: use the estimated stellar density to precisely constrain the  $a_k/R_*$  and  $P_k$  of the transiting planets observed in our transit lightcurves. Because the periods are usually precisely constrained by the periodicity of the transits, the stellar density therefore constrains  $a_k/R_*$  for transiting planets. Although stating all the benefits that such a constraint provides is outside the scope of this work, it is interesting to note that because the transit duration along with the ingress and egress times have information about the argument of periastron passage and the eccentricity of the orbit as well (see, e.g., Winn 2010), the stellar density constraint allows us, in principle, to extract part of this information from these observables (see, e.g., Kipping et al. 2012; Dawson & Johnson 2012; Kipping 2014, and references therein). Similarly, in the presence of grazing orbits, this parametrization allows us to break known degeneracies in the transit modelling for a precise estimation of the impact parameter — an effect that also manifestates itself on not very well sampled lightcurves (Kipping 2010). Because of all these benefits, *juliet* allows to optionally include any available estimate on the stellar density as input.

In practice, within *juliet* one can incorporate a measured stellar density into the modelling in two ways if there is only one transiting planet, and in only one way if there are multiple transiting planets. If there is only one transiting exoplanet, then one way in which we incorporate stellar density information is as was already introduced in Brahm et al. (2018), where the stellar density  $\rho_*$  with its associated error  $\sigma_{\rho_*}$  estimated from the modelling of the stellar observables is incorporated in the joint modelling as an extra dataset/datapoint,  $y^{\text{SD}}$ . In this case, the probabilistic model for  $y^{\text{SD}}$  is easy to derive, and is of the form

$$y^{\text{SD}} \sim \hat{\rho}_* + \epsilon_{\text{SD}}, \quad (10)$$

where  $\hat{\rho}_* = [(3\pi)/(GP_k^2)](a/R_*)^3$  is the model of the stellar density and  $\epsilon_{\text{SD}} \sim N(0, \sigma_{\rho_*})$ , where  $\sigma_{\rho_*}$  is the error on our estimate for the stellar density. In this case,  $y^{\text{SD}}$  is understood as an independent dataset to that of the photometry and radial-velocities and, as such, is easy to incorporate in the joint modelling of the data. The log-likelihood of the parameters  $\vec{\theta} = (a/R_*, P)^T$  implied by the probabilistic model in equation 10 in this case is simply the logarithm of the probability density function of a gaussian distribution with mean  $(\rho_* - \hat{\rho}_*)$  and variance  $\sigma_{\rho_*}^2$ .

The general case of  $k$  transiting exoplanets, however, is

considerably more complicated to model in the presence of stellar density information using this parametrization, because each planet would impose a different stellar density through  $a_k/R_*$ , and the star can only have one stellar density. Because of this, within *juliet* we have implemented the possibility to fit directly for the stellar density which, together with the period  $P_k$  for each planet, defines through Kepler’s law a value of  $a_k/R_*$  for each planet. This makes the general case of fitting  $k$  transiting exoplanets in the presence of stellar density information a much easier problem to solve. Within this formulation, the prior is given directly on the stellar density parameter, which is then used directly as a fitting parameter. *juliet* then internally uses the transformation  $a_k/R_* = [(\rho_* GP_k^2)/(3\pi)]^{1/3}$  to generate the transit models for each individual  $k$  transiting exoplanet. The advantage of this formulation is that this parametrization not only constrains the  $a_k/R_*$  given observed periodic transits, but it also reduces the number of fitting parameters by  $k - 1$  terms. This formulation is also very useful to constrain the properties of singly transiting exoplanets.

## 2.5 Dynamic, Importance and/or Nested Sampling

Having defined the probabilistic model *juliet* assumes for the data in the previous sections, we now turn to a brief description of the algorithms *juliet* uses to both perform posterior sampling in order to obtain the posterior distribution of the parameters  $\vec{\theta}$  given the data  $\mathcal{D}$ ,  $p(\vec{\theta}|\mathcal{D})$  and to estimate bayesian evidences  $Z_i = p(\mathcal{D}|M_i)$  for model comparison of each model  $M_i$  via the posterior odds,  $p(M_i|\mathcal{D})/p(M_j|\mathcal{D}) = (Z_i/Z_j)(p(M_i)/p(M_j))$ . Currently, *juliet* allows the user to select between three possible sampling schemes: nested sampling, importance nested sampling and dynamic nested sampling. For detailed overviews, we recommend Feroz et al. (2009), Feroz et al. (2013), and Buchner (2014) for a thorough review of nested and importance nested sampling algorithms, and Buchner (2014) and Speagle (2019) for a review on dynamic nested sampling. Our discussion here stems mainly from these references.

The main idea of classical nested sampling algorithms (Skilling 2004, 2009) is to estimate the bayesian evidence of a model,  $Z$ , by noting that defining the “prior volume” as  $X(\lambda) = \int_{\mathcal{L}(\vec{\theta}) > \lambda} p(\vec{\theta}) d\theta_1 d\theta_2 \dots d\theta_N$ , where  $\mathcal{L}(\vec{\theta}) = p(\mathcal{D}|\vec{\theta})$  is the likelihood function, the evidence, which is the integral of the likelihood over the prior  $p(\vec{\theta})$ , can be written as a one-dimensional integral of the likelihood over  $X$ , i.e.,

$$Z = \int_0^1 \mathcal{L}(\vec{\theta}) p(\vec{\theta}) d\theta_1 d\theta_2 \dots d\theta_N = \int_0^1 \mathcal{L}(X) dX. \quad (11)$$

To find the value of  $Z$  for the typical case in which the shape of the likelihood function is unknown, Monte-Carlo sampling methods are used in order to sequentially shrink the prior volume,  $X$ , by sampling points from the prior  $p(\vec{\theta})$ . In essence, nested sampling algorithms sample  $N_{\text{live}}$  points from this prior and sequentially replace in each iteration the live-point with the lowest likelihood by a new live point with a larger one. During each iteration, the bayesian evidence is updated by a difference  $\Delta Z$ , and the stopping/convergence criterion is defined through a user defined evidence tolerance  $\Delta z$  below which the algorithm is said to have converged.

While classical nested sampling simply reject samples



**Table 3.** List of parameters that define each of the noise models for both the radial-velocities (RVs) and photometry for instrument  $i$  supported by *juliet*. Note that in the case in which one global GP is fit to all photometric or RV instruments, only the jitter terms are different for each instrument. For details on each model, see text.

Parameter name	Units	Description
White noise model		
$\sigma_{w,i}$	ppm, m/s or km/s <sup>1</sup>	Jitter term.
Multi-dimensional squared-exponential kernel		
$\sigma_{w,i}$	ppm, m/s or km/s <sup>1</sup>	Jitter term.
$\sigma_{\mathcal{GP},i}$	ppm, m/s or km/s	Amplitude of the GP.
$\alpha_d$	—	Inverse (squared) length-scale parameter for dimension $d$ .
Exponential kernel		
$\sigma_{w,i}$	ppm, m/s or km/s <sup>1</sup>	Jitter term.
$\sigma_{\mathcal{GP},i}$	ppm, m/s or km/s	Amplitude of the GP.
$T_i$	—	Length-scale of the GP process.
Approximate Matern kernel		
$\sigma_{w,i}$	ppm, m/s or km/s <sup>1</sup>	Jitter term.
$\sigma_{\mathcal{GP},i}$	ppm, m/s or km/s	Amplitude of the GP.
$\rho_i$	—	Length-scale of the GP process.
Exponential times Approximate Matern kernel		
$\sigma_{w,i}$	ppm, m/s or km/s <sup>1</sup>	Jitter term.
$\sigma_{\mathcal{GP},i}$	ppm, m/s or km/s	Amplitude of the GP.
$T_i$	—	Length-scale of the exponential part of the GP process.
$\rho_i$	—	Length-scale of the (approximate) Matern part of the GP process.
Exp-sine-squared times squared-exponential kernel		
$\sigma_{w,i}$	ppm, m/s or km/s <sup>1</sup>	Jitter term.
$\sigma_{\mathcal{GP},i}$	ppm, m/s or km/s	Amplitude of the GP.
$\alpha_i$	—	Inverse length-scale of the squared-exponential part of the GP process.
$\Gamma_i$	—	Amplitude of the Exp-sine-squared part of the kernel.
$P_{\text{rot},i}$	—	Characteristic period of the GP.
Celerite quasi-periodic kernel		
$\sigma_{w,i}$	ppm, m/s or km/s <sup>1</sup>	Jitter term.
$B_i$	ppm, m/s or km/s	Amplitude of the GP.
$C_I$	—	Constant scaling term of the GP.
$L_i$	—	Characteristic time-scale of the GP.
$P_{\text{rot},i}$	—	Characteristic period of the GP.
Stochastic Harmonic Oscillator (SHO) kernel		
$\sigma_{w,i}$	ppm, m/s or km/s <sup>1</sup>	Jitter term.
$S_0$	—	Characteristic power of the SHO.
$\omega_0$	—	Characteristic frequency of the SHO.
$Q$	—	Quality factor of the SHO.

<sup>1</sup> If the noise model is defined for the photometry, input is expected to be in parts-per-million (ppm). If defined for the RVs, it is expected to be in the same units as the input RV data (m/s or km/s).

that do not meet the requirement of having larger likelihoods than the lowest likelihood sampled by the current set of live-points, importance nested sampling uses all the sampled points from the prior, assigning different weights to each sampled value, which in turn leads to a better usage of the sampling and consequently a much faster convergence (see Cameron & Pettitt 2013; Feroz et al. 2013, for details). Within *juliet* we have incorporated both of these sampling schemes through the **MultiNest** algorithm (Feroz et al. 2009, 2013) via the **PyMultiNest**<sup>8</sup> package (Buchner et al. 2014). This algorithm is very efficient especially for multi-modal distributions as it encloses the live-points within ellipsoids, which can eventually be disconnected when different modes are found, allowing to accomodate the algorithm for very complicated shapes of the posterior distribution (see, e.g., examples in Feroz et al. 2013). Within *juliet* we use the

default tuning parameters of **MultiNest**, which as shown in Feroz et al. (2013) allow to tackle a wide range of posteriors including distributions much more complicated than the ones one might expect when fitting photometry and radial-velocitys of exoplanets. In particular, the default value within *juliet* for  $\Delta z$  is the default set in **MultiNest** which is 0.5 (it is important to notice that this is *not* the error on the evidence — this is typically more than an order of magnitude smaller than this stopping value). The number of live-points is set to a default of 1000, but it can be defined by the user.

One of the main drawbacks of nested sampling algorithms such as **MultiNest** is that because they are focused on evidence calculations, the posterior distribution of the parameters  $p(\vec{\theta}|\mathcal{D})$  is only a by-product of the procedure, which in turn might not explore as efficiently as possible the parameter space. The main reason for the inability of nested samplers to focus on posterior samples is because the number of live points  $N_{\text{live}}$  is kept constant, and thus

<sup>8</sup> <https://github.com/JohannesBuchner/PyMultiNest>

the prior volume shrinkage rate (i.e., the shrinking rate of  $X$ ) is always the same. To solve this, [Higson et al. \(2017\)](#) proposed to dynamically change the number of live-points in order to change the focus of the algorithm during the run. This sampling scheme, called “dynamic” nested sampling, has been implemented by [Speagle \(2019\)](#) through the `dynesty`<sup>9</sup> library, which we also incorporate within `juliet`. Here, however, the convergence criteria is much more involved to define as it is not solely evidence based, but also based on how much of the posterior distribution has been explored. Within `juliet` we use the default criterion described in Section 3.4 of [Speagle \(2019\)](#), which is the one implemented in `dynesty`.

We refer the reader to [Buchner \(2014\)](#) for a discussion on the advantages of dynamic nested sampling over “regular” nested sampling, but at first order, we recommend selecting to use `MultiNest` for (importance) nested sampling or `dynesty` for dynamic nested sampling within `juliet` having the number of dimensions (i.e., the number of parameters to be fitted) in mind: in our experience, `MultiNest` works well up to  $\sim 20$ -dimensional problems. For this order of magnitude problems and/or larger, users should use `dynesty` which provides algorithms specifically designed to tackle such large-dimensional problems. Both algorithms offer multi-threading options that one can use within `juliet` (via OpenMPI for `MultiNest` and via internal `python` multi-threading options for `dynesty`), allowing thus to scale the speed of convergence on multiple-core machines for large high-dimensional problems.

## 2.6 Joint modelling, model selection and parameter estimation

Using the sampling methods described in Section 2.5 and the probabilistic models described in previous sections, `juliet` allows to perform a joint modelling of transits and radial-velocities. We allow for all the possibilities: both transiting and non-transiting systems, and systems that can and cannot be detected via radial-velocities (which, of course, include the possible fitting of only transits and only radial-velocities). In practice, this implies we need to define the priors for our parameters (which are user-defined) and the likelihood function, which in our case is easy to compute as the sum of the individual log-likelihoods defined for the photometry and radial-velocities, which have the form defined in equation (3) plus the likelihood for the stellar density defined in the previous sub-section if one uses this as a datapoint. This latter term is of course not used if the stellar density is used as a parameter in the fit.

It is important to discuss the advantages and caveats that nested samplers offer for both model selection and parameter estimation, which is one of the main differences between `juliet` and other codes for analyzing photometric and radial-velocity measurements for the interpretation of exoplanetary signals. As it was briefly discussed above, nested sampling algorithms are specifically made for the estimation of bayesian evidences of different models given the data,  $Z_i$ , which in turn provide us with a useful tool for model selection. However, it is important to highlight that

model evidences are heavily impacted by the priors used to estimate them and, thus, special care must be taken when selecting them. Also of importance are the errors on the evidences quoted by nested sampling algorithms. According to the recent work of [\(Nelson et al. 2018\)](#), at least for cases in which one is performing both parameter estimation and model selection on radial-velocity only datasets they seem to be underestimated, and thus care must be taken on this front when comparing evidences between different models. In our experience with `juliet`, however, having transits and radial-velocities being fitted simultaneously significantly leverages this problem, as the periodic nature of transits precisely constrain the ephemerides of the exoplanetary signals. Although providing an extensive analysis such as the one of [Nelson et al. \(2018\)](#) when it comes to model comparison and selection in datasets with both transits and radial-velocities is out the scope of this work, this possibility should still be kept in mind. We thus echo the recommendations in [Nelson et al. \(2018\)](#): to run a handful of `juliet` runs when comparing model evidences in different cases to check for consistency between the estimates of the bayesian evidences provided by the nested sampling algorithm under use.

In terms of parameter estimation, nested samplers offer a very important advantage: given a thorough exploration of the prior volume is needed in order to compute model evidences, nested sampling algorithms are very efficient at thoroughly exploring the parameter space, and thus, on the search for not only the global optimum but also for local minima which might be true solutions of a possibly multi-modal posterior distribution. Given proper priors, this provides a very efficient venue to search for the optimal parameters during the posterior distribution exploration simultaneously. This property is unlike Markov-Chain Monte Carlo (MCMC) algorithms such as the classical Metropolis-Hastings algorithms (see, e.g., the discussion in [Tak et al. 2018](#)) or of widely used fast algorithms such as `emcee` ([Foreman-Mackey et al. 2013](#)) which require initial guesses of the parameters to be made in order to attain convergence in a reasonable amount of time. This is especially important for posterior exploration of models using GPs, for which a search of optimal parameters before posterior exploration is usually a tough task to optimize in itself. Of course, the larger the prior volume the slower the convergence of nested sampling algorithms as well — however, the multi-threading capabilities of the nested sampling algorithms used within `juliet`, can help in leveraging this issue for typical problems in exoplanetary science.

## 3 MODELLING PLANETARY SYSTEMS WITH `juliet`

Having defined the probabilistic models and sampling capabilities `juliet` offers in the past sections, here we showcase some of the features `juliet` offers for the analysis of transiting and non-transiting exoplanetary systems. In order to do this, we perform a detailed analysis of two interesting systems. First, we perform a thorough analysis of the K2-140b system, which is a hot-Jupiter that has been claimed to have a significant eccentricity in [Giles et al. \(2018\)](#). This claim, however, has been put into question by the analysis in [Korth et al. \(2019\)](#). We believe this system is interest-

<sup>9</sup> <https://github.com/joshspeagle/dynesty>

ing for us to showcase the power *juliet* has for providing a quantitative view not only into the question of whether a given dataset supports or not the presence of a property such as a significant eccentricity, but also to illustrate the interpretation of dilution factors, how *juliet* handles whether GPs are needed to account for additional systematics in the data and how stellar density priors impact on the analysis of a system. After this analysis, we perform an analysis of the K2-32 multi-planet system, whose radial-velocities have been analyzed in [Petigura et al. \(2017\)](#) but for which a joint analysis has not been presented in the literature so far. For the analysis of the K2-140 system we use *MultiNest*, as the number of parameters in all of our analyses are on the order of 20 free parameters. For the analysis of the K2-32 system we use *dynesty*, as in this case the number of free parameters is larger (30). In what follows and following [Trotta \(2008\)](#), we consider  $\Delta \ln Z = 2$  (or posterior odds of  $\approx 7 : 1$ , assuming equiprobable models) as a threshold between weak and moderate evidence that one model is preferred over the other, whereas  $\Delta \ln Z = 5$  (or posterior odds of  $\approx 150 : 1$  assuming equiprobable models) as strong evidence of one model over the other. We have run all the examples below several times and have found that the (log-)evidence estimates have errors  $\lesssim 0.1$ ; we thus don't quote values for the evidences smaller than this.

### 3.1 Analyzing the K2-140 system with *juliet*

The data used here for K2-140 considers (1) the K2 photometry, (2) follow-up photometry from the Las Cumbres Observatory Global Telescope (LCOGT) Network, (3) radial-velocities from CORALIE and HARPS (photometric and radial-velocity data already introduced in [Giles et al. 2018](#)) and (4) radial-velocities from the FIES instrument, introduced in [Korth et al. \(2019\)](#). This dataset, along with the scripts used to generate the analysis to be presented in this Section (including sampling parameters such as, e.g., the number of live-points) are made available in the *juliet* Github wiki page<sup>10</sup>.

#### 3.1.1 Photometric analyses with *juliet*

We first analyze the photometry of K2-140b using *juliet*. First of all, we must consider the fact that the K2 photometry for K2-140 was obtained in the long-cadence mode of K2 photometry, which if not accounted for can give rise to biases in the retrieved transit parameters ([Kipping 2010](#)). As such, we account for this effect within *juliet* by supersampling the lightcurve using the *Kepler* exposure time (0.020434 days), and super-sampling  $N = 20$  datapoints at each K2 time-step, averaging these datapoints in order to generate our model lightcurve. Inside *juliet*, this process is easily defined by flags the user can give before starting a *juliet* run. In practice, the supersampling is actually performed by *batman* ([Kreidberg 2015](#)), which is the transit modelling tool *juliet* uses to generate the transit models. In addition, following [Espinoza & Jordán \(2016\)](#) we use a

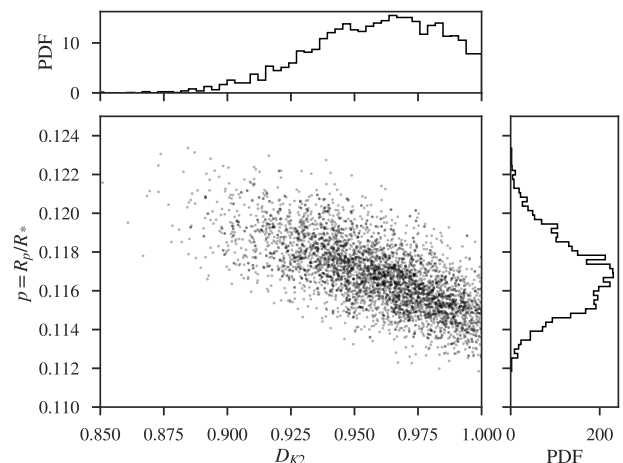


**Figure 1.** Posterior distribution of the dilution factor for the K2 photometry versus the planet-to-star radius ratio for K2-140b. Note how the correlation between the parameters enlarges the posterior distribution of the planet-to-star radius ratio.

quadratic limb-darkening law for the precise K2 photometry and a linear law for the less precise LCOGT photometry; these are also easily defined via flags within *juliet*.

#### 3.1.2 Dilution factors

As a first fit to the data, we try a white-noise analysis to the K2 photometry and LCOGT photometry simultaneously assuming a circular orbit and letting all the parameters have the wide uninformative priors presented in Table 4. In order to decide whether we should include the dilution factors and on which instruments, we try turning off the dilutions of each instrument. The retrieved log-evidence indicates that the best model of those is one in which we fix the dilution to 1 for both instruments ( $\Delta \ln Z > 2$  for this model when compared against all the other models). All the other models are statistically indistinguishable from one another (all have  $\Delta \ln Z < 2$  between themselves). One might, however, have good reason to believe a-priori that the best would be to leave the dilution factor for the K2 photometry as a free parameter in the fit, as the *Kepler* pixels are relatively large ( $\sim 4''$ ) and, indeed, the aperture used to extract the K2 photometry might include light from nearby sources that could be diluting the transit.

In Figure 1 we present the posterior distribution of the dilution factor for the K2 photometry versus the planet-to-star radius ratio for the case in which the LCOGT photometry dilution factor is fixed to 1 (which is a reasonable assumption as the aperture used to obtain this photometry is on the order of arcseconds), and in which it can be seen how the correlation between these two parameters enlarges the posterior distribution of the latter making its marginal posterior more uncertain. It is interesting to interpret what this dilution factor *means* in light of our discussion in Section 2.1. As it was discussed in that section, we can interpret the dilution factor as a measure of the light that is being added

<sup>10</sup> <https://github.com/nespinoza/juliet/wiki>

to the aperture by other sources; i.e.,

$$\sum_n F_n/F_T = \frac{1-D}{D}.$$

In our case,  $\sum_n F_n/F_T = 4.2^{+3.1}_{-2.6}\%$ . Multiplying this by -2.51 and taking the logarithm base 10, we find that if this dilution was indeed made by a nearby star, this would imply a star with a delta-magnitude  $\Delta m = 3.5^{+1.0}_{-0.6}$  fainter than the target star; in general,  $n$  sources of magnitudes  $\Delta m = 2.51 \log_{10}(n) + 3.5^{+1.0}_{-0.6}$  can produce such a dilution. Looking at nearby stars around K2-140 (i.e., stars within  $\sim 4$  *Kepler* pixels or  $\sim 16$  arcseconds to it) in Gaia DR2 (Gaia Collaboration et al. 2018), we see that there is only one source (Gaia ID: 3579426058019822080) that *might* add flux to the K2 aperture used to obtain the photometry of K2-140. However, this source is much too faint ( $\Delta G = 8.7$  fainter than the target star, which has  $G = 12.48$ ) to produce this level of dilution. Given that the field does not seem to be especially crowded according to the Gaia detections around 10 arcminutes of the target (441 sources down to  $G = 21$ , or around 1.4 sources per arcminute<sup>2</sup>), it seems very unlikely that there are undetected sources blended with K2-140 that could give rise to the level of dilution implied by our K2 observations when leaving this parameter be free in the fit. A close exploration of the posterior distribution of the parameters reveals that the increase in the width of the marginal posterior distribution of the planet-to-star radius ratio is due to the limb-darkening coefficients, which in this case have a strong correlation with both this parameter and the dilution factor (which makes sense, as those parameters heavily influence on the shape of the transit lightcurve). Based on our evidence calculation and in our posterior information regarding close-by sources, we thus decide to use the simpler model suggested by our log-evidence calculations, in which the dilution factors of both of our instruments are set to unity in what follows.

### 3.1.3 Gaussian Processes

As discussed in Section 2.1, *juliet* is able to fit GPs given any external parameters to each photometric instrument in order to account for possible systematic effects. The K2 photometry presented in Giles et al. (2018) has already been detrended and as such we do not bother to try a GP on that dataset, but we might believe that the LCOGT photometry might need some systematics correction. To test this, we model any systematic trends in the LCOGT photometry with a simple squared-exponential kernel in time, setting a prior of  $\sigma_{\mathcal{GP}, \text{LCOGT}} \sim \mathcal{J}(1, 10^4)$  and  $\alpha_{\hat{t}, \text{LCOGT}} \sim \mathcal{J}(0.01, 10)$  for this instrument, where  $\hat{t}$  is the time subtracted by its mean and divided by its standard deviation (i.e., we standardize the time variable). These parameters are added to the priors defined in Table 4, and as was discussed in Section 3.1.2 we fix the dilution factors to 1 for both instruments.

The resulting evidences for the GP and no-GP fits with *juliet* reveal that the evidence for both models are statistically indistinguishable ( $\Delta \ln Z < 1$ ); however, the no-GP model's evidence is actually larger than the GP model. As such, we decide to use the model without this GP in time. We show the resulting fits of this photometric *juliet* analysis in Figure 2.

### 3.1.4 Radial-velocity analyses with *juliet*

We now analyze the radial-velocities with *juliet*, in order to showcase the features our code provides for the analysis of this kind of data. We perform two analyses: one in which we first consider ourselves agnostic as to whether there is a planetary signal in the radial-velocity data or not, and another one in which we use the ephemerides obtained for our photometric analysis in the previous sub-section in order to search for evidence of eccentricity in the radial velocities.

For our “agnostic” analysis, we perform a *juliet* run with the priors presented in Table 5. As a null model, we perform an analysis using the same priors for all the parameters but the jitters, whose priors we set from 0.1 to 1000 m/s, and the planetary elements, where we fix the semi-amplitude to zero. This analysis provides ample evidence for a planetary signal when compared against the null model: the evidence for the planetary model is  $\Delta \ln Z = 10$  larger than for the null model (i.e., the planetary model is 4 orders of magnitude larger than the null model). In turn, the period and time of transit center(s) we obtain with our analysis,  $t_0 = 2457588.40 \pm 0.58$  (obtained subtracting 48 times the best-fit period to match the time-of-transit center of the K2 observations),  $P = 6.566 \pm 0.015$ , whose joint posterior distribution is presented in Figure 3, perfectly agrees with the ephemerides observed in the transit data, for which we obtained  $t_0 = 2457588.28379 \pm 0.00026$  and  $P = 6.569301 \pm 0.000029$ . It is important to notice that this latter distribution is multi-modal for obvious reasons: a time of transit plus or minus  $nP$  is also a solution to the problem. However, not all the modes are equally precise: the most precise in terms of the time-of-transit center is, in fact, the one in the middle of the observing window. Modes farther away from this get more and more horizontal in the  $(t_0, P)$ -plane, meaning the correlations between  $t_0$  and  $P$  is stronger. This makes sense as to predict the next time-of-transit center one has to add  $n$  times the period  $P$ , making future and past predictions of the time-of-transit center much more imprecise and correlated with  $P$ . This in turn showcases one of the features that *juliet* provides thanks to the nested sampling algorithms it uses: it easily handles multi-modal distributions.

Having ample evidence for a planetary signal in the radial-velocities, we now turn to our analysis on the search for evidence of eccentricity in the radial-velocity dataset only. For this, we use the same priors as the ones presented in Table 5, but now use as priors on the ephemerides of the orbit the period and time-of-transit center found with our photometric-only analysis. In addition to this, we fit for  $S_1 \sim \mathcal{U}(-1, 1)$  and  $S_2 \sim \mathcal{U}(-1, 1)$  in the eccentric case, and set the eccentricity to 0 in the circular case.

The results of our analysis are presented in Figure 4. In terms of the retrieved evidences, our results are ambiguous: the eccentric model has a log-evidence only  $\Delta \ln Z = 0.20$  larger than the circular model, which makes both models statistically indistinguishable. From Figure 4 we can visually see that this reflects exactly what we observe when comparing the circular and eccentric fits given the data at hand — there is no evident improvement on the fits when inspecting either the residuals of the circular or eccentric model fit. Using only the radial-velocities, thus, it is impossible to determine if the system is indeed eccentric or not: given this



**Table 4.** Priors used in the analysis of the photometry for K2-140b. Here  $p = R_p/R_*$  and  $b = (a/R_*)\cos(i_p)$ , where  $R_p$  is the planetary radius,  $R_*$  the stellar radius,  $a$  the semi-major axis of the orbit and  $i_p$  the inclination of the planetary orbit with respect to the plane of the sky.  $e$  and  $\omega$  are the eccentricity and argument of periastron of the orbits.  $\mathcal{N}(\mu, \sigma^2)$  represents a normal distribution of mean  $\mu$  and variance  $\sigma^2$ .  $\mathcal{U}(a, b)$  represents a uniform distribution between  $a$  and  $b$ .  $\mathcal{J}(a, b)$  represents a Jeffrey’s prior (i.e., a log-uniform distribution) between  $a$  and  $b$ .

Parameter name	Prior	Units	Description
Parameters for K2-140b			
$P_b$	$\mathcal{N}(6.5693, 0.01^2)$	days	Period of K2-140b.
$t_{0,b}$	$\mathcal{N}(2457588.28380, 0.01^2)$	days	Time of transit-center for K2-140b.
$a_b/R_*$	$\mathcal{U}(1, 30)$	stellar radii	Scaled semi-major axis for K2-140b.
$r_{1,b}$	$\mathcal{U}(0, 1)$	—	Parametrization <sup>1</sup> of Espinoza (2018) for $p$ and $b$ for K2-140b.
$r_{2,b}$	$\mathcal{U}(0, 1)$	—	Parametrization <sup>1</sup> of Espinoza (2018) for $p$ and $b$ for K2-140b.
Parameters for K2 photometry			
$D_{K2}$	$\mathcal{U}(0, 1)$	—	Dilution factor for K2.
$M_{K2}$	$\mathcal{N}(0, 0.1^2)$	relative flux	Relative flux offset for K2.
$\sigma_{w,K2}$	$\mathcal{J}(0.1, 500^2)$	relative flux (ppm)	Extra jitter term for K2 lightcurve.
$q_{1,K2}$	$\mathcal{U}(0, 1)$	—	Quadratic limb-darkening parametrization <sup>3</sup> (Kipping 2013).
$q_{2,K2}$	$\mathcal{U}(0, 1)$	—	Quadratic limb-darkening parametrization <sup>3</sup> (Kipping 2013).
Parameters for LCOGT photometry			
$D_{LCOGT}$	$\mathcal{U}(0, 1)$	—	Dilution factor for LCOGT.
$M_{LCOGT}$	$\mathcal{N}(0, 0.1^2)$	relative flux	Relative flux offset for LCOGT.
$\sigma_{w,LCOGT}$	$\mathcal{J}(0.1, 5000^2)$	relative flux (ppm)	Extra jitter term for LCOGT lightcurve.
$q_{1,LCOGT}$	$\mathcal{U}(0, 1)$	—	Linear limb-darkening coefficient for the LCOGT photometry.

<sup>1</sup> To perform the transformation between the  $(r_1, r_2)$  plane and the  $(b, p)$  plane, we performed the transformations outlined in Espinoza (2018) depending on the values of  $r_1$  and  $r_2$ : with  $p_l = 0$  and  $p_u = 1$ , if  $r_1 > A_r = (p_u - p_l)/(2 + p_l + p_u)$ , then  $(b, p) = ([1 + p_l][1 + (r_1 - 1)/(1 - A_r)], (1 - r_2)p_l + r_2p_u)$ . If  $r_1 \leq A_r$ , then  $(b, p) = ([1 + p_l] + \sqrt{r_1/A_r}r_2(p_u - p_l), p_u + (p_l - p_u)\sqrt{r_1/A_r}[1 - r_2])$ .

<sup>3</sup> To transform from the  $(q_1, q_2)$  plane to the plane of the quadratic limb-darkening coefficients,  $(u_1, u_2)$ , we use the transformations outlined in Kipping (2013) for this law  $u_1 = 2\sqrt{q_1}q_2$  and  $u_2 = \sqrt{q_1}(1 - 2q_2)$ .

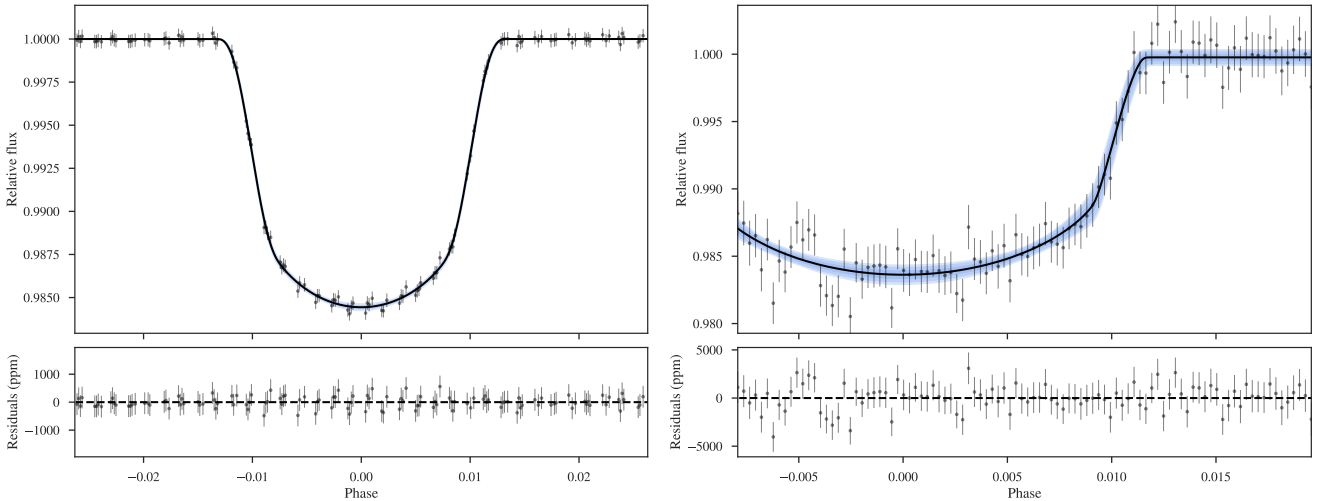


**Figure 2.** Lightcurve fits of our *juliet* run on the photometry for K2-140b (left, K2 photometry; right, LCOGT photometry). The errorbars include the fitted photometric jitter terms added in quadrature. Solid black lines show our best-fit models; blue bands denote 68, 95 and 99% posterior credibility bands for our best-fit models.

data only and the priors used, both the circular and eccentric models are indistinguishable.

### 3.1.5 Joint-analyses with *juliet*

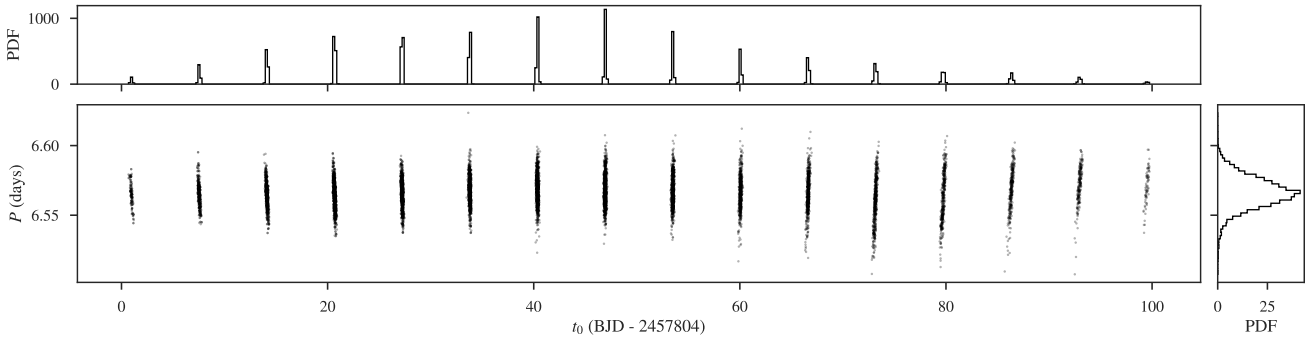
We now turn to the final analysis of the K2-140 dataset, on which we perform joint analyses of the photometry and

radial-velocities with *juliet* in order to showcase the impact this kind of analysis have on helping constrain the planetary parameters from this data. We perform two joint analyses here: one in which we ignore the stellar parameters, and one in which we incorporate the stellar density information into our modelling.

For our first set of analyses, we perform a joint analysis of the photometry and radial-velocities with *juliet*

**Table 5.** Priors used in the “agnostic” radial-velocity analysis of the K2-140 system using `juliet` on the search for evidence in the RVs for radial-velocity variations on K2-140 due to K2-140b. A circular orbit is assumed.

Parameter name	Prior	Units	Description
Parameters for K2-140b			
$P_b$	$\mathcal{J}(0.1, 100)$	days	Period of K2-140b.
$t_{0,b}$	$\mathcal{U}(2457803, 2457905)$	days	Time of transit-center for K2-140b.
$K_b$	$\mathcal{U}(0, 1000)$	m/s	Radial-velocity semi-amplitude for K2-140b.
RV parameters			
$\mu_{\text{CORALIE}}$	$\mathcal{N}(1220, 50^2)$	m/s	Systemic velocity for CORALIE.
$\sigma_{w,\text{CORALIE}}$	$\mathcal{J}(0.1, 100)$	m/s	Extra jitter term for CORALIE.
$\mu_{\text{HARPS}}$	$\mathcal{N}(1240, 50^2)$	m/s	Systemic velocity for HARPS.
$\sigma_{w,\text{HARPS}}$	$\mathcal{J}(0.1, 100)$	m/s	Extra jitter term for HARPS.
$\mu_{\text{FIES}}$	$\mathcal{N}(1215, 50^2)$	m/s	Systemic velocity for FIES.
$\sigma_{w,\text{FIES}}$	$\mathcal{J}(0.1, 100)$	m/s	Extra jitter term for FIES.

**Figure 3.** Posterior distribution of the time of transit center and period of the orbit of our “agnostic” analysis. This distribution showcases one of the features of nested samplers: their ability to sample from a posterior with multiple-modes.

using the priors defined in Table 6. For the priors in the ephemerides of our joint fit, we inflated the uncertainties found from our photometry-only analysis. Our joint fitting of the data reveals plots very similar to the ones already presented in Figures 2 and 4; however, the difference between the evidences of both the circular and eccentric fits are slightly different: we obtain a  $\ln Z = 0.6$  in favor of the eccentric model. Although formally both models are indistinguishable, it is interesting to see the slight increase in the evidence in this case when compared with the radial-velocity only dataset, which might be a product of the increased information the transit photometry gives to the final orbits. This, however, has a null impact on the actual posterior distributions of the eccentricity and argument of periastron, which is virtually the same as the ones we observe for the case in which we fit for the radial-velocity dataset only.

We now perform the same fits just described, but including the stellar density information of K2-140 on our analysis, following our discussion in Section 2.4. For this, we use the procedures described in Brahm et al. (2018). Briefly, we first determine the stellar atmospheric parameters from publicly available HARPS spectra using the `zasp` code (Brahm et al. 2017). We then use a spectral energy distribution model from Baraffe et al. (2015) having the atmospheric parameters found with `zasp`, the public available photometry for K2-140, and its Gaia DR2 parallax (Gaia Collaboration et al. 2018) to determine its stellar

radius through an mcmc code<sup>11</sup>. Finally, we compute the stellar mass and age by using the Yonsei-Yale stellar evolutionary models (Yi et al. 2001), which are compared to the spectroscopic effective temperature and the stellar radius via another mcmc code<sup>12</sup>. With this procedure we obtained precise stellar parameters for K2-140 which are presented in Table 7. In particular, we use the estimate of the stellar density in the likelihood method presented in Section 2.4 to incorporate this information into our modelling. Within `juliet`, this is also easily done by adding a flag to the `juliet` runs. We tried the same fits using  $\rho_*$  as a parameter instead of  $a/R_*$  (a method also discussed in Section 2.4), and obtain the same results as the ones we present here.

Adding the stellar density information into our analysis significantly changes the evidence for eccentricity in the K2-140 system: we obtain a  $\Delta \ln Z = 1.7$  in favor of a *circular* orbit. Although, again, given the current data both models are indistinguishable, it is interesting to see how the addition of the stellar density significantly changes the evidence now *in favor of a circular orbit*. In fact, this addition of the stellar density significantly changes the distribution of the eccentricity and argument of periastron between the eccentric joint fit using and not using the stellar density information. We show the posterior distribution of these parameters for

<sup>11</sup> <https://github.com/rabrahm/rstar><sup>12</sup> <https://github.com/rabrahm/isoAR>

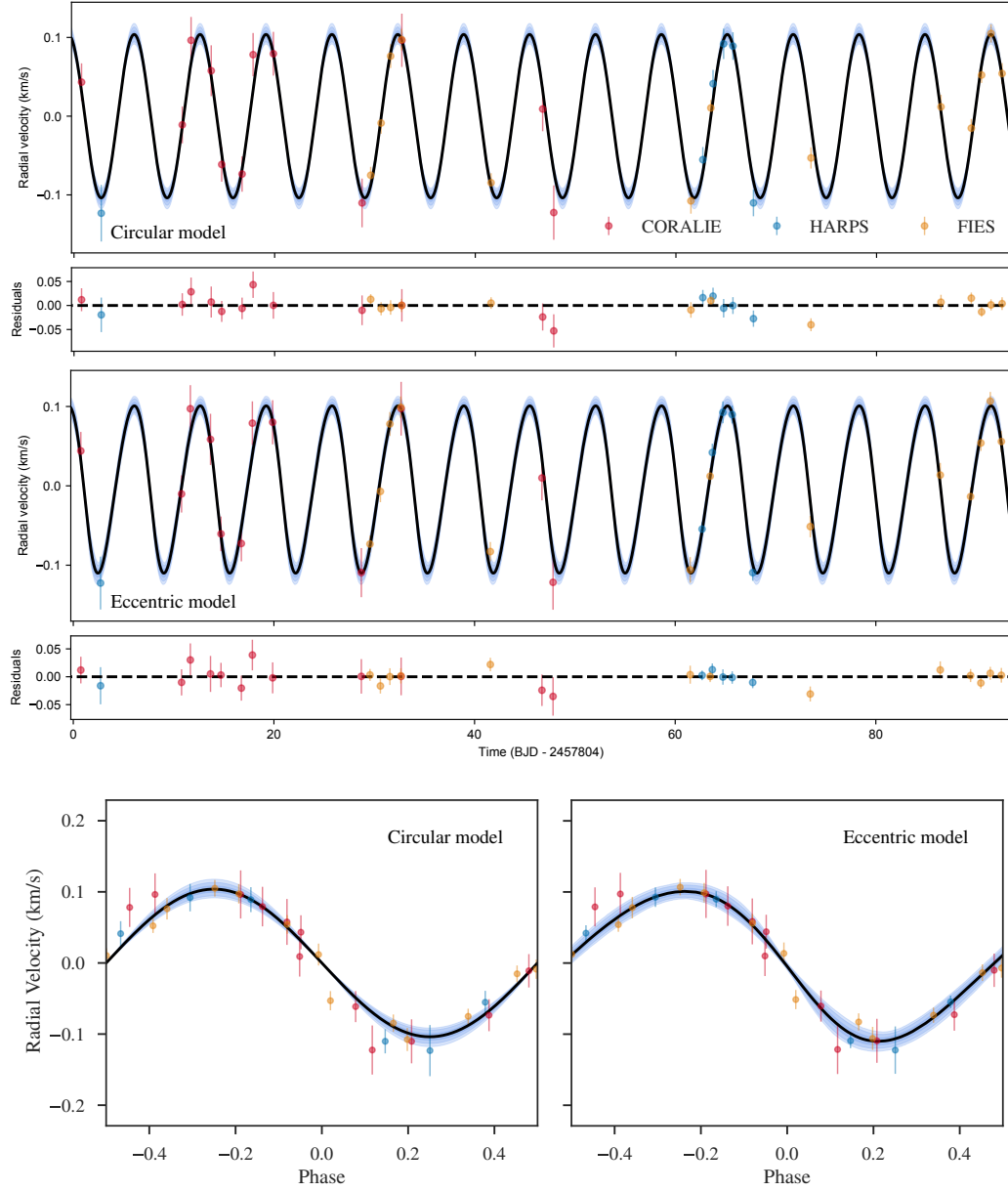


**Figure 4.** Radial-velocity fits for K2-140b both using a circular (upper panels and lower left panel) and an eccentric (upper panels and lower right panel) model. According to the analysis of the bayesian evidences, both models are indistinguishable from one another (see text).

both cases in Figure 5. The impact that the stellar density information has on constraining the eccentricity and argument of periastron using transits has already been made aware by various researchers in the past (see, e.g., [Kipping et al. 2012](#); [Dawson & Johnson 2012](#); [Kipping 2014](#), and references therein) and has already been discussed in length in Section 2.4; however, its impact on the joint analysis of transits and radial-velocities has only recently been started to be exploited thanks to the precise absolute stellar parameters that precision spectroscopy combined with the Gaia mission ([Gaia Collaboration et al. 2018](#)) provides, and is a property one can take advantage of using *juliet*. It is interesting to discuss how in Figure 5 part of the parameter space in eccen-

tricity and the argument of periastron using the stellar density is no longer consistent with the values obtained when not using this information. This can be explained as the stellar density information gives strong information about the duration of the transit (through a strong definition of the parameter  $a/R_*$ ), which in turn constrains the possible velocities the planet can acquire based on the transit information. This information in turn significantly reduces the parameter space  $e$  and  $\omega$  can occupy in the posterior.

Our results regarding the eccentric nature of the K2-140b system using all the available information (photometry, radial-velocities and the stellar density) is, thus, not evident given the data: both models are statistically indis-

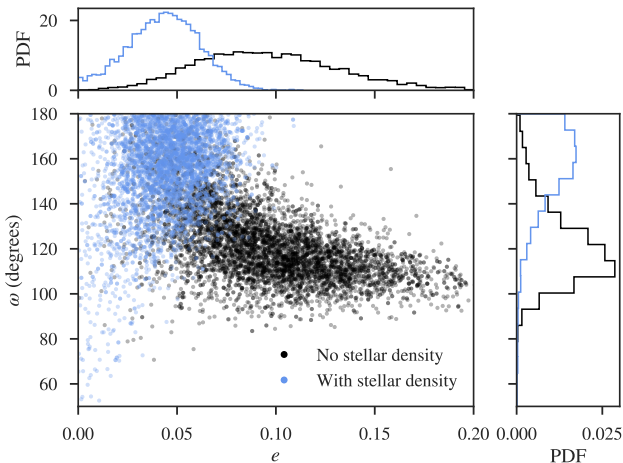
**Table 6.** Priors used in our joint analysis of the K2-140 system using *juliet*.

Parameter name	Prior	Units	Description
Parameters for K2-140b			
$P_b$	$\mathcal{N}(6.5693, 0.0001^2)$	days	Period of K2-140b.
$t_{0,b}$	$\mathcal{N}(2457588.284, 0.001^2)$	days	Time of transit-center for K2-140b.
$a_b/R_*$	$\mathcal{U}(1, 30)$	stellar radii	Scaled semi-major axis for K2-140b.
$r_{1,b}$	$\mathcal{U}(0, 1)$	—	Parametrization <sup>1</sup> of Espinoza (2018) for $p$ and $b$ for K2-140b.
$r_{2,b}$	$\mathcal{U}(0, 1)$	—	Parametrization <sup>1</sup> of Espinoza (2018) for $p$ and $b$ for K2-140b.
$S_{1,b} = \sqrt{e_b} \sin \omega_b$	$\mathcal{U}(-1, 1)$	—	Parametrization <sup>2</sup> for $e$ and $\omega$ for K2-140b.
$S_{2,b} = \sqrt{e_b} \cos \omega_b$	$\mathcal{U}(-1, 1)$	—	Parametrization <sup>2</sup> for $e$ and $\omega$ for K2-140b.
$K_b$	$\mathcal{U}(0, 1000)$	m/s	Radial-velocity semi-amplitude for K2-140b.
Parameters for K2 photometry			
$D_{K2}$	1 (fixed)	—	Dilution factor for K2.
$M_{K2}$	$\mathcal{N}(0, 0.1^2)$	relative flux	Relative flux offset for K2.
$\sigma_{w,K2}$	$\mathcal{J}(0.1, 500^2)$	relative flux (ppm)	Extra jitter term for K2 lightcurve.
$q_{1,K2}$	$\mathcal{U}(0, 1)$	—	Quadratic limb-darkening parametrization <sup>3</sup> (Kipping 2013).
$q_{2,K2}$	$\mathcal{U}(0, 1)$	—	Quadratic limb-darkening parametrization <sup>3</sup> (Kipping 2013).
Parameters for LCOGT photometry			
$D_{LCOGT}$	1 (fixed)	—	Dilution factor for LCOGT.
$M_{LCOGT}$	$\mathcal{N}(0, 0.1^2)$	relative flux	Relative flux offset for LCOGT.
$\sigma_{w,LCOGT}$	$\mathcal{J}(0.1, 5000^2)$	relative flux (ppm)	Extra jitter term for LCOGT lightcurve.
$q_{1,LCOGT}$	$\mathcal{U}(0, 1)$	—	Linear limb-darkening coefficient for the LCOGT photometry.
RV parameters			
$\mu_{CORALIE}$	$\mathcal{N}(1220, 50^2)$	m/s	Systemic velocity for CORALIE.
$\sigma_{w,CORALIE}$	$\mathcal{J}(0.1, 100)$	m/s	Extra jitter term for CORALIE.
$\mu_{HARPS}$	$\mathcal{N}(1240, 50^2)$	m/s	Systemic velocity for HARPS.
$\sigma_{w,HARPS}$	$\mathcal{J}(0.1, 100)$	m/s	Extra jitter term for HARPS.
$\mu_{FIES}$	$\mathcal{N}(1215, 50^2)$	m/s	Systemic velocity for FIES.
$\sigma_{w,FIES}$	$\mathcal{J}(0.1, 100)$	m/s	Extra jitter term for FIES.

<sup>1</sup> To perform the transformation between the  $(r_1, r_2)$  plane and the  $(b, p)$  plane, we performed the transformations outlined in Espinoza (2018) depending on the values of  $r_1$  and  $r_2$ : with  $p_l = 0$  and  $p_u = 1$ , if  $r_1 > A_r = (p_u - p_l)/(2 + p_l + p_u)$ , then  $(b, p) = ([1 + p_l][1 + (r_1 - 1)/(1 - A_r)], (1 - r_2)p_l + r_2p_u)$ . If  $r_1 \leq A_r$ , then  $(b, p) = ([1 + p_l] + \sqrt{r_1/A_r}r_2(p_u - p_l), p_u + (p_l - p_u)\sqrt{r_1/A_r}[1 - r_2])$ .

<sup>2</sup> We ensure in each sampling iteration that  $e = S_1^2 + S_2^2 \leq 1$ .

<sup>3</sup> To transform from the  $(q_1, q_2)$  plane to the plane of the quadratic limb-darkening coefficients,  $(u_1, u_2)$ , we use the transformations outlined in Kipping (2013) for this law  $u_1 = 2\sqrt{q_1}q_2$  and  $u_2 = \sqrt{q_1}(1 - 2q_2)$ .

**Figure 5.** Posterior distribution for the eccentricity and argument of periastron from our joint fits both using (blue) and not (black) the information on the stellar density. Note how this significantly changes the posterior distributions of these quantities.**Table 7.** Stellar parameters for K2-140.

Atmospheric parameters	
$T_{\text{eff}}$ (K)	$5736^{+49}_{-45}$
$\log g$	$4.479^{+0.016}_{-0.012}$
Fe/H	$0.20 \pm 0.04$
$v \sin i$	$2.65 \pm 0.20$
Absolute stellar parameters	
$M_*$ ( $M_{\odot}$ )	$1.077^{+0.020}_{-0.019}$
$R_*$ ( $R_{\odot}$ )	$0.991^{+0.015}_{-0.016}$
$L_*$ ( $L_{\odot}$ )	$0.952^{+0.053}_{-0.052}$
$\rho_*$ (cgs)	$1.565^{+0.079}_{-0.063}$
Age (Gyr)	$1.10^{+0.75}_{-1.09}$
$M_V$	$4.883^{+0.065}_{-0.071}$

tinguishable ( $\ln Z < 2$ ). However, given the circular model is the simpler of the two, we can conclude that this appears to be the best model given the data at hand. More data is needed, however, to confidently rule out a significant ec-



**Table 8.** Posterior parameters obtained from our joint photometric and radial-velocity *juliet* analysis for K2-140b (including stellar density information).

Parameter name	Posterior estimate <sup>a</sup>
Posterior parameters for K2-140b	
$P_b$	$6.569298^{+0.000026}_{-0.000027}$
$t_{0,b}$ (BJD UTC)	$2457588.28381^{+0.00024}_{-0.00024}$
$a_b/R_*$	$15.24^{+0.13}_{-0.16}$
$r_{1,b}$	$0.402^{+0.054}_{-0.047}$
$r_{2,b}$	$0.11437^{+0.00083}_{-0.00087}$
$K_b$ (m/s)	$103.8^{+4.8}_{-4.5}$
$e_b$	0 (fixed <sup>b</sup> , < 0.078)
Posterior parameters for K2 photometry	
$M_{K2}$ (ppm)	$-35.5^{+8.4}_{-8.0}$
$\sigma_{w,K2}$ (ppm)	$381.7^{+5.7}_{-5.7}$
$q_{1,K2}$	$0.213^{+0.127}_{-0.075}$
$q_{2,K2}$	$0.57^{+0.22}_{-0.18}$
Posterior parameters for LCOGT photometry	
$M_{LCOGT}$ (ppm)	$230^{+230}_{-220}$
$\sigma_{w,LCOGT}$ (ppm)	$18.8^{+122.5}_{-16.3}$
$q_{1,LCOGT}$	$0.586^{+0.064}_{-0.065}$
Posterior RV parameters	
$\mu_{CORALIE}$ (m/s)	$1214.9^{+7.5}_{-7.9}$
$\sigma_{w,CORALIE}$ (m/s)	$1.16^{+5.3}_{-0.9}$
$\mu_{HARPS}$ (m/s)	$1246.6^{+7.3}_{-8.0}$
$\sigma_{w,HARPS}$ (m/s)	$13.5^{+10.3}_{-9.3}$
$\mu_{FIES}$ (m/s)	$1131.8^{+3.6}_{-3.6}$
$\sigma_{w,FIES}$ (m/s)	$1.6^{+6.7}_{-1.4}$
Derived transit parameters for K2-140b	
$R_p/R_*$	$0.11437^{+0.00083}_{-0.00087}$
$b = (a/R_*) \cos(i_p)$	$0.104^{+0.081}_{-0.071}$
$i_p$ (deg)	$89.60^{+0.27}_{-0.31}$

<sup>a</sup> Errorbars denote the 68% posterior credibility intervals.

<sup>b</sup> Upper limits denote the 95% upper credibility interval of fits when allowing the orbit to be eccentric.

centricity for K2-140b. The final transit and radial-velocity parameters obtained with our joint fit to the data are presented in Table 8.

### 3.2 A *juliet* view of the multi-planetary system around K2-32

We now turn our attention to the K2-32 system, a system observed during Campaign 2 of the K2 mission in long-cadence mode, which we will model using *juliet* in order to showcase various of the features that the code can handle, including the fact that it can efficiently fit multi-planetary systems using data from several instruments. For this system, we retrieved the radial velocities used in [Petigura et al. \(2017\)](#) which includes radial-velocities obtained in that work and in

[Dai et al. \(2016\)](#). For the K2 photometry, we retrieved the photometry reduced with the EVEREST pipeline ([Luger et al. 2016, 2018b](#)) using K2DD<sup>13</sup>. The EVEREST lightcurves maintain any systematic and astrophysical signal in the photometry that is unique to the target, and thus this photometry is very useful to showcase the ability of *juliet* to model these features (which we here model with a GP) along with the transit parameters and the radial-velocity measurements. As with the K2-140b system, the scripts to perform the analyses presented in this section are also given in *juliet*'s Github wiki page<sup>14</sup>.

K2-32 is a system composed of three exoplanets in a nearly resonant chain with periods of 9, 21 and 32 days ([Petigura et al. 2017](#)). In order to model it with *juliet*, we now thus use the stellar density as a fitting parameter instead of  $a/R_*$  for each planet which, as discussed in Section 2.4, is the most efficient way of incorporating the stellar density information in the fit for multi-planetary systems. We used the same method as the one for K2-140 described in the previous sub-section to estimate the stellar density of K2-32 to be  $\rho_* = 2094 \pm 82 \text{ kg/m}^3$ . We fix the dilution factor to unity as the dilution from nearby sources based on the Gaia detections around 16" arcseconds from the target ( $\sim 4$  K2 pixels) would all produce dilutions  $1 > D > 0.99$  in  $G$ , which we assume would be similar to the expected dilution in the *Kepler* bandpass.

We tried different GP kernels to account for the long-term trend observed in the K2-32 *Kepler* photometry: an exponential kernel, the approximate Matern kernel introduced in [Foreman-Mackey et al. \(2017\)](#), a multiplication of those two kernels and the quasi-periodic kernel introduced in equation (9). We performed four model fits in total with wide priors for all parameters and found via the posterior evidence that the best model is the one that uses the multiplication of the exponential kernel with the approximate Matern. This makes sense with our intuition when looking at the light curve (presented in Figure 6): there are not evident quasi-periodic oscillations and thus it was unlikely for a quasi-periodic kernel to be a good fit to the data in our case. On the other hand, either only an exponential or only a Matern kernel would be too strict to account for both short term and longer-term trends observed in the data. It is interesting to note, however, that all the fits gave rise to very similar posterior parameters for the physical properties of the system (all within 1-sigma), which hints that in this case the selection of the *exact*, "best" kernel does not impact too much on the results — it will, however, most likely impact on posterior predictions outside of the range of the time-series. We summarize all the priors used for the analysis of this system for this best-fit scenario in Table 9. For simplicity and ease of comparison, we assume a circular orbit as was assumed in [Petigura et al. \(2017\)](#) — a full analysis including evidence of eccentric orbits is left for future work. In total, we seek the posterior distribution of 29 free parameters, and as discussed in the introduction of this section, we thus use *dynesty* to perform this fit. As with K2-140b, we also account for the long-cadence integrations by

<sup>13</sup> <http://github.com/nespinoza/k2DD>

<sup>14</sup> <https://github.com/nespinoza/juliet/wiki>

supersampling the transit lightcurve with  $N = 20$  resamples per point with the same exposure time used for K2-140b.

Figures 6, 7 and 8 show the results of our joint fit to the data, which reveals an excellent fit to the whole dataset. As can be observed in Figure 6, the GP we used to account for the long-term trend captures perfectly well the observed long-term trend in the K2 photometry. We show the phased transits of the exoplanets K2-32b, K2-32c and K2-32d after subtracting this GP component from the data in Figure 7. In Figure 8 we present the radial-velocity component of our joint fit, which shows a very similar shape as the radial-velocity only analysis presented in [Petigura et al. \(2017\)](#). As can be seen, thus, *juliet* can efficiently fit multi-planetary systems.

We present the resulting posterior parameters of the system with our *juliet* joint fit in Tables 10 and 11. Comparing our posterior parameters with the ones published by [Petigura et al. \(2017\)](#), we see that we obtain values in excellent agreement albeit more precise than that previous work. This is most likely a result of the fact that our joint analysis including the stellar density provides more precise timing ephemerides, which in turn lets us obtain more precise values for the semi-amplitudes of the planets in the system.

## 4 DISCUSSION

As was presented in Section 3, *juliet* is a very flexible code that allows to incorporate a variety of setups in the analysis of photometry, radial-velocity or both, for both transiting and non-transiting systems, as was illustrated with our analysis of the K2-140 system in Section 3.1 and the multi-planetary system around K2-32b in Section 3.2. It is efficient both at exploring wide parameter spaces, and also at providing quantitative measures of evidence of adding or not extra parameters/models on the fits (e.g., dilution factors, GPs, eccentricity, additional planets in the system). In this Section, we discuss and explore how the features provided by *juliet* can be used in the analysis of other datasets, along with a discussion on the speed of the library in different settings.

### 4.1 GP hyperparameter sharing within *juliet*

In Sections 3.1 and 3.2, we showed how GPs can be introduced to different instruments independently in the photometry. However, one feature we did not present here but which is also available within *juliet* is that, as explained in Sections 2.1 and 2.2, the hyperparameters of these kernels can be shared not only with a GP being incorporated in the radial-velocity dataset, but they can also be shared *between* photometric datasets as well. This feature of *juliet* has been used in [Luque et al. \(2019\)](#), for example, to estimate the rotation period of the star GJ 357 using photometry from different ground-based instruments which were fit with a quasi-periodic kernel, where the characteristic period and time-scale of the process were common to all instruments, but the amplitudes and jitter terms were not (due to, e.g., different passbands). This allowed to retrieve a very precise estimate of this parameter which was critical for the study of the stellar properties and their relation to activity. If in addition to these datasets a radial-velocity dataset

is also used where signatures of rotational modulation are either suspected or observed, a GP can also be fit simultaneously to the radial-velocities which, as already mentioned, can in turn also share said hyperparameters of the photometric GPs. We believe this kind of joint analyses are not only important for transiting exoplanets, but could also be key for radial-velocity analyses in order to correctly propagate the information between the photometry and the radial-velocities in a consistent way, especially in cases where the rotation period of stars (usually estimated through photometric rotational modulation) are very close, fractions, or at the periods of suspected planets in radial-velocity analyses (see, e.g., [Tuomi et al. 2018](#); [Díaz et al. 2018](#)).

### 4.2 *juliet* as a planet detection tool

As it was briefly introduced in Section 3.1.4, *juliet* can also be used as a planet detection tool similar to *kima*, a tool presented by [Faria et al. \(2018\)](#) for the detection of exoplanets in radial-velocity datasets. *kima*, however, is more efficient than *juliet* at this task as it includes the number of planets in the system as a free parameter itself, performing thus one fit instead of the many fits for different models that one has to perform with *juliet*. However, the versatility *juliet* offers in terms of kernel types for modelling stellar activity might make it a good competitor. Indeed, *juliet* has already been used in [Espinoza et al. \(2019\)](#), [Kossakowski et al. \(2019\)](#), [Brahm et al. \(2019\)](#) and [Luque et al. \(2019\)](#) to search for additional planets in radial-velocities, tightly constraining the presence of at least three planets in the latter work. *juliet* might also be seen as more versatile in the sense that it can not only handle different instruments but also transits, if available, which in turn can help not only constrain a subset of the suspected exoplanets in the system embedded in a given radial-velocity dataset if their transits are observed in the photometry, but also help in the search for evidence of transiting exoplanets in photometric data alone. This latter usage of *juliet* has already been introduced in [Espinoza et al. \(2019\)](#) when searching for transits of TOI-141c, and we believe it might be interesting to compare against simpler (but faster) algorithms such as the widely used Box-Least Squares (BLS; [Kovács et al. 2002](#)) algorithm. In particular, it will be interesting to test if the error underestimation of the bayesian evidences discussed in [Nelson et al. \(2018\)](#) when quantifying the evidence of additional planets in radial-velocity datasets is also a problem on the search for additional planets in transit photometry.

### 4.3 Computing speed of *juliet*

In this work we have made many analyses with *juliet* but we have not discussed yet how much it takes for the fits to converge (see Section 2.5), which might be one of the key points that might define whether one wants to use *juliet* or other open source tools like the ones discussed in the introduction of this manuscript for the problem at hand. In general, the smaller the prior, the faster the algorithm will converge for obvious reasons already discussed in Section 2.5. On this front, it is important to note that in this work we deliberately tried very wide priors for all the parameters to showcase the ability of nested samplers to properly explore the whole parameter space. Most of the analyses made

**Table 9.** Priors used in our joint analysis of the K2-32 multi-planetary system using *juliet*. The GP used for the K2 photometry was an exponential multiplied by an approximate Matern kernel, both of which were introduced in Section 2.1.

Parameter name	Prior	Units	Description
Parameters for K2-32			
$\rho_*$	$\mathcal{N}(2094, 82^2)$	kg/m <sup>3</sup>	Stellar density of K2-32.
Parameters for K2-32b			
$P_b$	$\mathcal{N}(6.5693, 0.0001^2)$	days	Period of K2-32b.
$t_{0,b}$	$\mathcal{N}(2457588.284, 0.001^2)$	days	Time of transit-center for K2-32b.
$r_{1,b}$	$\mathcal{U}(0, 1)$	—	Parametrization <sup>1</sup> of Espinoza (2018) for $p$ and $b$ for K2
$r_{2,b}$	$\mathcal{U}(0, 1)$	—	Parametrization <sup>1</sup> of Espinoza (2018) for $p$ and $b$ for K2
$K_b$	$\mathcal{U}(0, 100)$	m/s	Radial-velocity semi-amplitude for K2-32b.
Parameters for K2-32c			
$P_c$	$\mathcal{N}(6.5693, 0.0001^2)$	days	Period of K2-32c.
$t_{0,c}$	$\mathcal{N}(2457588.284, 0.001^2)$	days	Time of transit-center for K2-32c.
$r_{1,c}$	$\mathcal{U}(0, 1)$	—	Parametrization <sup>1</sup> of Espinoza (2018) for $p$ and $b$ for K2
$r_{2,c}$	$\mathcal{U}(0, 1)$	—	Parametrization <sup>1</sup> of Espinoza (2018) for $p$ and $b$ for K2
$K_c$	$\mathcal{U}(0, 100)$	m/s	Radial-velocity semi-amplitude for K2-32c.
Parameters for K2-32d			
$P_d$	$\mathcal{N}(6.5693, 0.0001^2)$	days	Period of K2-32d.
$t_{0,d}$	$\mathcal{N}(2457588.284, 0.001^2)$	days	Time of transit-center for K2-32d.
$r_{1,d}$	$\mathcal{U}(0, 1)$	—	Parametrization <sup>1</sup> of Espinoza (2018) for $p$ and $b$ for K2
$r_{2,d}$	$\mathcal{U}(0, 1)$	—	Parametrization <sup>1</sup> of Espinoza (2018) for $p$ and $b$ for K2
$K_d$	$\mathcal{U}(0, 100)$	m/s	Radial-velocity semi-amplitude for K2-32d.
Parameters for K2 photometry			
$D_{K2}$	1 (fixed)	—	Dilution factor for K2.
$M_{K2}$	$\mathcal{N}(0, 0.1^2)$	relative flux	Relative flux offset for K2.
$\sigma_{w,K2}$	$\mathcal{J}(1, 1000^2)$	relative flux (ppm)	Extra jitter term for K2 lightcurve.
$q_{1,K2}$	$\mathcal{U}(0, 1)$	—	Quadratic limb-darkening parametrization <sup>3</sup> (Kipping 2013)
$q_{2,K2}$	$\mathcal{U}(0, 1)$	—	Quadratic limb-darkening parametrization <sup>3</sup> (Kipping 2013)
Parameters for the GP of K2 photometry			
$\sigma_{K2}$	$\mathcal{J}(0.1, 10^4)$	ppm	Amplitude of the GP.
$T_{K2}$	$\mathcal{J}(0.02, 10^5)$	days	Time-scale of the exponential part of the kernel.
$\rho_{K2}$	$\mathcal{J}(0.02, 10^5)$	days	Time-scale of the Matern part of the kernel.
RV parameters			
$\mu_{\text{HIRES}}$	$\mathcal{N}(0, 10^2)$	m/s	Systemic velocity for HIRES.
$\sigma_{w,\text{HIRES}}$	$\mathcal{J}(0.01, 10)$	m/s	Extra jitter term for HIRES.
$\mu_{\text{HARPS}}$	$\mathcal{N}(0, 10^2)$	m/s	Systemic velocity for HARPS.
$\sigma_{w,\text{HARPS}}$	$\mathcal{J}(0.01, 10)$	m/s	Extra jitter term for HARPS.
$\mu_{\text{PFS}}$	$\mathcal{N}(0, 10^2)$	m/s	Systemic velocity for PFS.
$\sigma_{w,\text{PFS}}$	$\mathcal{J}(0.01, 10)$	m/s	Extra jitter term for PFS.

<sup>1</sup> To perform the transformation between the  $(r_1, r_2)$  plane and the  $(b, p)$  plane, we performed the transformations outlined in Espinoza (2018) depending on the values of  $r_1$  and  $r_2$ : with  $p_l = 0$  and  $p_u = 1$ , if  $r_1 > A_r = (p_u - p_l)/(2 + p_l + p_u)$ , then  $(b, p) = ([1 + p_l][1 + (r_1 - 1)/(1 - A_r)], (1 - r_2)p_l + r_2p_u)$ . If  $r_1 \leq A_r$ , then  $(b, p) = ([1 + p_l] + \sqrt{r_1/A_r}r_2(p_u - p_l), p_u + (p_l - p_u)\sqrt{r_1/A_r}[1 - r_2])$ .

<sup>2</sup> We ensure in each sampling iteration that  $e = \mathcal{S}_1^2 + \mathcal{S}_2^2 \leq 1$ .

<sup>3</sup> To transform from the  $(q_1, q_2)$  plane to the plane of the quadratic limb-darkening coefficients,  $(u_1, u_2)$ , we use the transformations outlined in Kipping (2013) for this law  $u_1 = 2\sqrt{q_1}q_2$  and  $u_2 = \sqrt{q_1}(1 - 2q_2)$ .

in this work were performed using a laptop with an Intel(R) Core(TM) i5-7287U CPU at 3.30GHz. In this laptop, for single photometry and/or radial-velocity analyses *juliet* takes of order of minutes depending on the complexity of the fit. For multiple-instrument photometry or radial-velocity fits without the inclusion of GPs, *juliet* takes on the order of minutes to converge with the standard *MultiNest* and *dynesty* options built in within *juliet*. When GPs are included, the runs tested here took on the order of tens of minutes to converge.

For joint analyses of photometry and radial-velocities, for a single planetary system with only one instrument and no GPs, *juliet* takes tens of minutes to run. However, as

the dimensions and complexity of the problems increase, the computing speed increases as well. For example, the K2-140b full analysis presented in Section 3.1 took several hours to converge in the laptop mentioned above, and we found, as expected, that the speed of convergence strongly depends on the priors (larger priors take longer to converge). As a rule of thumb, problems with dimensions of order  $\sim 20$  take several hours (depending on the complexity of the problem, e.g., if several GPs are included in the fit it could take of order a day in a laptop like the one defined above). However, when approaching these large number of dimensions, users might want to use the multi-threading capabilities *juliet* provides through *MultiNest* and *dynesty*. For example, the full fit of

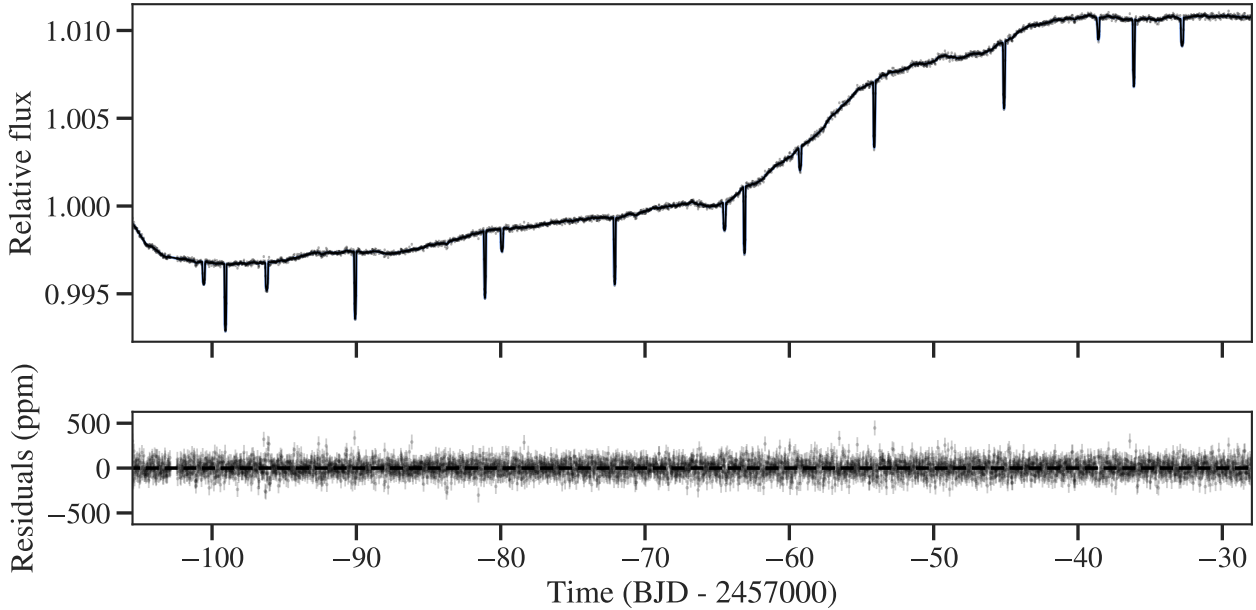


**Figure 6.** Top panel. Full K2 photometry (datapoints with errorbars) for the K2-32 multi-planet system obtained with the `EVEREST` algorithm (Luger et al. 2016, 2018b). The solid black line indicates the photometric fit component of our `juliet` joint fit to the data, which includes both the transits of the exoplanets K2-32b, K2-32c and K2-32d and the GP used to account for the observed long-term trend. Bottom panel. Residuals of our photometric fit.

the K2-32 system detailed in Section 3.2, which includes 29 free parameters and a GP in time to model the K2 systematics took only 1 hour when `juliet` was ran in multi-threading mode using `dynesty` with 10 cores on a Intel(R) Xeon(R) CPU E5-2699 v3 at 2.30GH machine. Within `juliet` multi-threading for `dynesty` can be included with a simple flag that determines the number of threads one wants to use. Via `MultiNest`, direct support of OpenMPI is available as `PyMultiNest` automatically recognizes this call.

## 5 CONCLUSIONS AND FUTURE WORK

In this work we have presented a new versatile open source code, `juliet`, with which one can perform efficient fitting of photometry, radial-velocity or both, allowing the user to not only thoroughly explore the parameter space but which also provides estimates for the bayesian model evidence (thanks to nested sampling algorithms), with which one can formally perform model comparison. Using two previously analyzed systems, K2-140b (Giles et al. 2018; Korh et al. 2019) and K2-32b (see Petigura et al. 2017, and references therein), we have shown how `juliet` is versatile enough to allow for multiple-instruments, dilutions, GPs and even multi-planetary systems to be efficiently fit, allowing in turn to answer questions in terms of, e.g., the evidence of eccentricity in a given dataset, the best kernel to use for a GP in a given dataset or even the presence of additional signals both in transits and in radial-velocities. As such, `juliet` is a versatile tool for the characterization of extrasolar planets that we believe will prove to be very useful in the *TESS* era of planet discovery.

Our plans for future work are multiple. In the near-future, we plan to incorporate support for secondary eclipses

which can easily be implemented within `batman` (Kreidberg 2015), and thus allow users to optionally include this effect in the joint and/or photometric fitting with `juliet`. We also plan to incorporate within `juliet` other codes that allow to model a plethora of other photometric effects such as `starry` (Luger et al. 2018a) and/or `spiderman` (Louden & Kreidberg 2018). This would in turn transform `juliet` into a characterization toolbox which will not only be able to discover the exoplanets under study, but also shine some light on what these exoplanets are made of.

On the front of GP regression, we aim at implementing GP kernels on request. We have made sure to incorporate in this first version of `juliet` the most popular GP kernels in use but it might happen that other kernels gain popularity in the near future. Implementing new kernels within `juliet` is relatively easy given the excellent work that has been made on the packages used by the code to implement GPs (`george` and `celerite`) and as such we believe that not only us but the community could perform their own kernel implementations and push them to the `juliet` Github repository.

We note that a full documentation for `juliet` has been published alongside this paper<sup>15</sup>.

## ACKNOWLEDGEMENTS

We would like to thank the referee, Daniel Foreman-Mackey, for very useful suggestions that greatly improved the paper and the `juliet` library. N.E. would like to thank the Gruber Foundation for its generous support to this research. N.E. would like to thank J. Buchner and J. Speagle for useful

<sup>15</sup> <https://juliet.readthedocs.io/en/latest/>



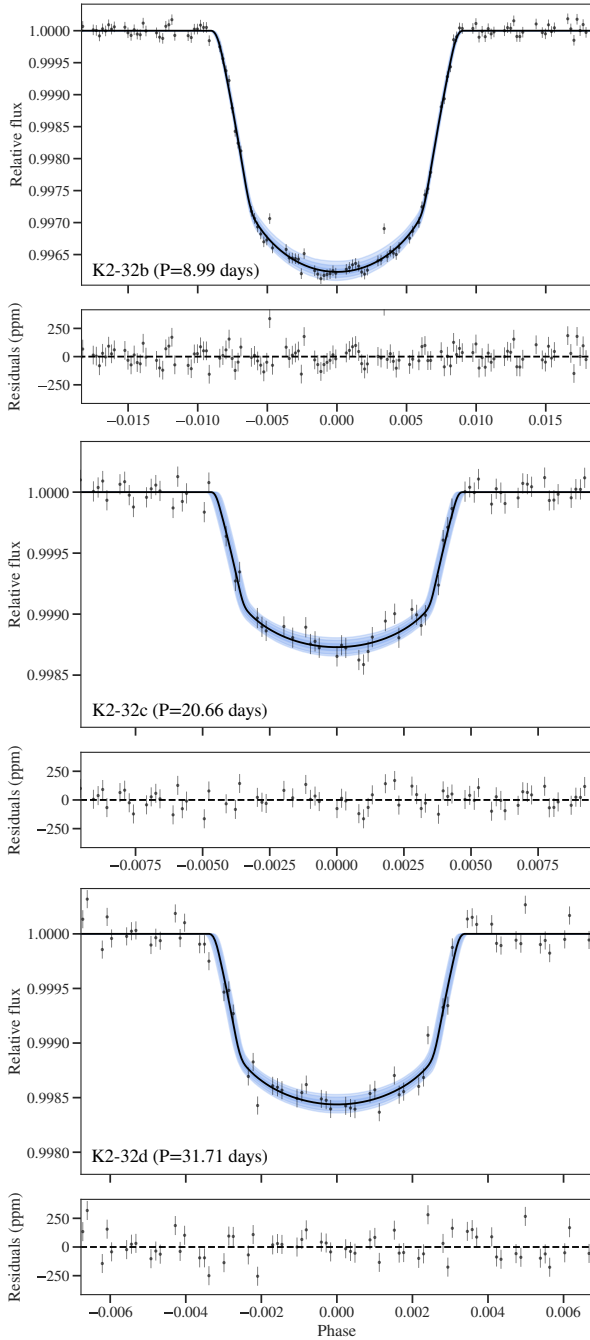


**Figure 7.** Phased transits after removing the GP component from the K2 photometry for K2-32b (top), K2-32c (middle) and K2-32d (bottom).

discussions regarding the usage of MultiNest and *dynesty*, respectively. N.E. and D.K. would like to thank M. Gunther and T. Daylan for fruitful discussions on the topics discussed in this article and T. Trifonov and the CARMENES team on discussions regarding the analysis of radial-velocities. R.B. acknowledges support from FONDECYT Post-doctoral Fellowship Project 3180246, and from the Millennium Institute of Astrophysics (MAS).

## REFERENCES

- Ambikasaran S., Foreman-Mackey D., Greengard L., Hogg D. W., O’Neil M., 2014
- Arriagada P., 2011, *ApJ*, **734**, 70
- Bakos G. Á., 2018, preprint, ([arXiv:1801.00849](https://arxiv.org/abs/1801.00849))
- Bakos G. Á., et al., 2010, *ApJ*, **710**, 1724
- Baluev R. V., 2013, *Astronomy and Computing*, **2**, 18
- Baluev R. V., 2018, *Astronomy and Computing*, **25**, 221
- Baraffe I., Homeier D., Allard F., Chabrier G., 2015, *A&A*, **577**, A42
- Barragán O., Gandolfi D., Antoniciello G., 2019, *MNRAS*, **482**, 1017
- Borucki W. J., et al., 2010, *Science*, **327**, 977
- Bouchy F., et al., 2009, *A&A*, **505**, 853
- Brahm R., Jordán A., Hartman J., Bakos G., 2017, *MNRAS*, **467**, 971
- Brahm R., et al., 2018, preprint, ([arXiv:1806.04073](https://arxiv.org/abs/1806.04073))
- Brahm R., et al., 2019, *AJ*, **158**, 45
- Buchner J., 2014, preprint, [p. arXiv:1407.5459](https://arxiv.org/abs/1407.5459) ([arXiv:1407.5459](https://arxiv.org/abs/1407.5459))
- Buchner J., et al., 2014, *A&A*, **564**, A125
- Burdanov A., Delrez L., Gillon M., Jehin E., Speculoos T., Trappist Teams 2017, SPECULOOS Exoplanet Search and Its Prototype on TRAPPIST. p. 130, [doi:10.1007/978-3-319-30648-3\\_130-1](https://doi.org/10.1007/978-3-319-30648-3_130-1)
- Butler R. P., et al., 2017, *AJ*, **153**, 208
- Cameron E., Pettitt A., 2013, arXiv e-prints, [p. arXiv:1301.6450](https://arxiv.org/abs/1301.6450)
- Dai F., et al., 2016, *ApJ*, **823**, 115
- Dawson R. I., Johnson J. A., 2012, *ApJ*, **756**, 122
- Díaz R. F., Almenara J. M., Santerne A., Moutou C., Lethuillier A., Deleuil M., 2014, *MNRAS*, **441**, 983
- Díaz M. R., et al., 2018, *AJ*, **155**, 126
- Eastman J., 2017, EXOFASTv2: Generalized publication-quality exoplanet modeling code, Astrophysics Source Code Library ([ascl:1710.003](https://ui.adsabs.org/abs/2017ASCl..1710.003))
- Eastman J., Gaudi B. S., Agol E., 2013, *PASP*, **125**, 83
- Eastman J. D., et al., 2019, arXiv e-prints, [p. arXiv:1907.09480](https://arxiv.org/abs/1907.09480)
- Espinoza N., 2018, *Research Notes of the AAS*, **2**, 209
- Espinoza N., Jordán A., 2015, *MNRAS*, **450**, 1879
- Espinoza N., Jordán A., 2016, *MNRAS*, **457**, 3573
- Espinoza N., et al., 2016, *ApJ*, **830**, 43
- Espinoza N., et al., 2019, arXiv e-prints, [p. arXiv:1903.07694](https://arxiv.org/abs/1903.07694)
- Faria J. P., Santos N. C., Figueira P., Brewer B. J., 2018, *The Journal of Open Source Software*, **3**, 487
- Feroz F., Hobson M. P., Bridges M., 2009, *MNRAS*, **398**, 1601
- Feroz F., Hobson M. P., Cameron E., Pettitt A. N., 2013, arXiv e-prints, [p. arXiv:1306.2144](https://arxiv.org/abs/1306.2144)
- Ford E. B., 2006, *ApJ*, **642**, 505
- Foreman-Mackey D., Hogg D. W., Lang D., Goodman J., 2013, *PASP*, **125**, 306
- Foreman-Mackey D., Agol E., Ambikasaran S., Angus R., 2017, *AJ*, **154**, 220
- Foreman-Mackey D., Barentsen G., Barclay T., 2019, *dfm/exoplanet: exoplanet v0.1.6*, [doi:10.5281/zenodo.2651251](https://doi.org/10.5281/zenodo.2651251), <https://doi.org/10.5281/zenodo.2651251>
- Fulton B. J., Petigura E. A., Blunt S., Sinukoff E., 2018, *PASP*, **130**, 044504
- Gaia Collaboration et al., 2018, *A&A*, **616**, A1
- Gazak J. Z., Johnson J. A., Tonry J., Dragomir D., Eastman J., Mann A. W., Agol E., 2012, *Advances in Astronomy*, **2012**, 697967
- Gibson N. P., 2014, *MNRAS*, **445**, 3401
- Gibson N. P., Aigrain S., Roberts S., Evans T. M., Osborne M., Pont F., 2012, *MNRAS*, **419**, 2683
- Giles H. A. C., et al., 2018, *MNRAS*, **475**, 1809
- Günther M. N., Daylan T., 2019, *allesfitter: Flexible star and exoplanet inference from photometry and radial velocity*, As-

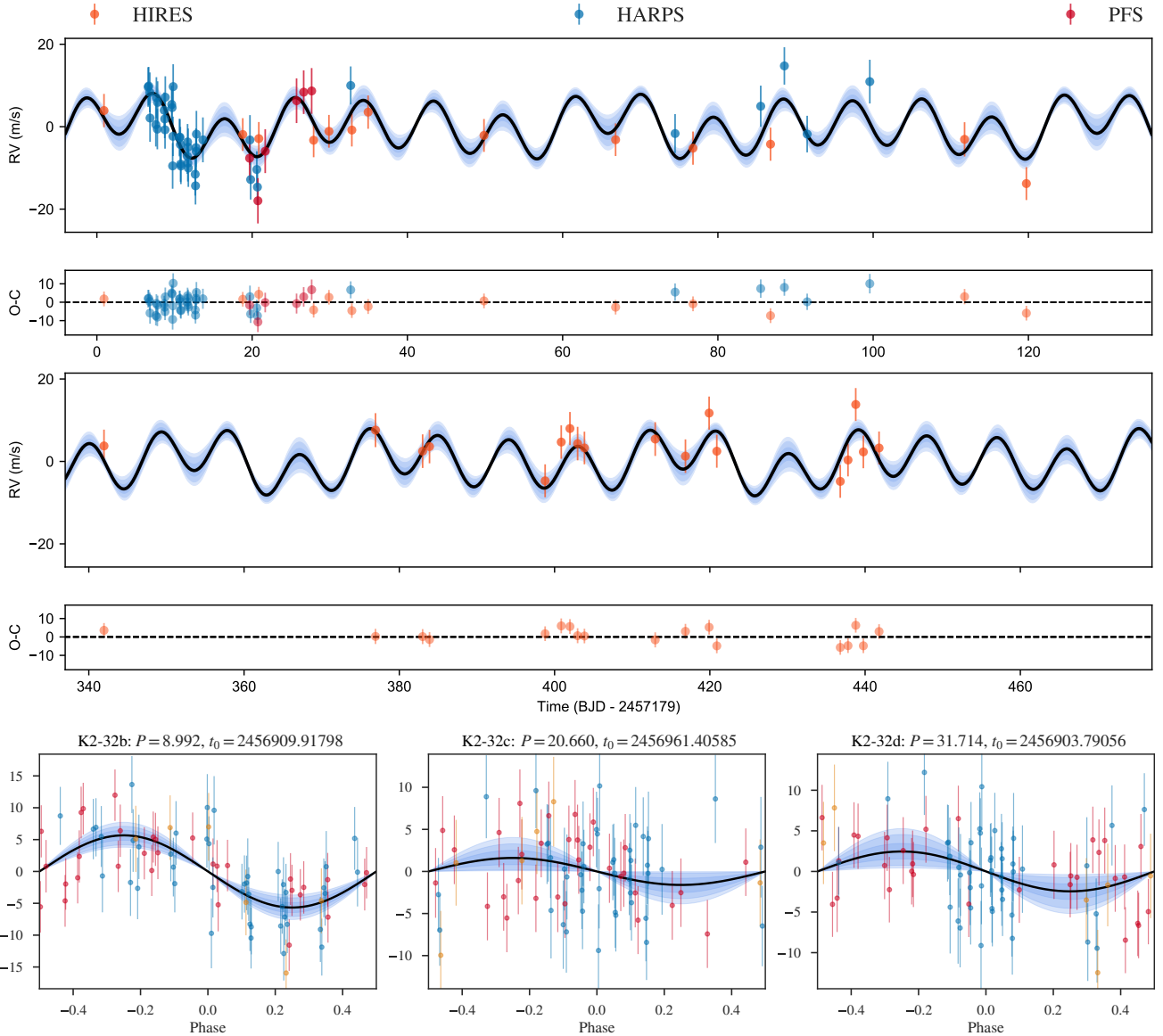


**Figure 8.** Radial-velocity component of our *juliet* fit to the data of the K2-32 multi-planetary system. The top panel shows the radial-velocities as a function of time and the bottom panels shows the phased radial-velocities after removing the radial-velocity component from the other planets.

trophyphysics Source Code Library (ascl:1903.003)  
Hartman J. D., et al., 2009, *ApJ*, **706**, 785  
Hartman J. D., et al., 2012, *AJ*, **144**, 139  
Hartman J. D., et al., 2018, preprint, [p. arXiv:1809.01048](https://arxiv.org/abs/1809.01048)  
(arXiv:1809.01048)  
Haywood R. D., et al., 2014, *MNRAS*, **443**, 2517  
Higson E., Handley W., Hobson M., Lasenby A., 2017, arXiv e-prints, [p. arXiv:1704.03459](https://arxiv.org/abs/1704.03459)  
Howarth I. D., 2011, *MNRAS*, **418**, 1165  
Iglesias-Marzoa R., López-Morales M., Jesús Arévalo Morales M., 2015, *Publications of the Astronomical Society of the Pacific*, **127**, 567  
Kipping D. M., 2010, *MNRAS*, **408**, 1758  
Kipping D. M., 2013, *MNRAS*, **435**, 2152  
Kipping D. M., 2014, *MNRAS*, **440**, 2164  
Kipping D. M., Tinetti G., 2010, *MNRAS*, **407**, 2589  
Kipping D. M., Dunn W. R., Jasinski J. M., Manthri V. P., 2012,

*MNRAS*, **421**, 1166  
Korth J., et al., 2019, *MNRAS*, **482**, 1807  
Kossakowski D., et al., 2019, arXiv e-prints, [p. arXiv:1906.09866](https://arxiv.org/abs/1906.09866)  
Kovács G., Zucker S., Mazeh T., 2002, *A&A*, **391**, 369  
Kreidberg L., 2015, *PASP*, **127**, 1161  
Kürster M., Trifonov T., Reffert S., Kostogryz N. M., Rodler F., 2015, *A&A*, **577**, A103  
Laughlin G., 2003, in Deming D., Seager S., eds, *Astronomical Society of the Pacific Conference Series Vol. 294*, Scientific Frontiers in Research on Extrasolar Planets. pp 189–192  
Louden T., Kreidberg L., 2018, *MNRAS*, **477**, 2613  
Luger R., Agol E., Kruse E., Barnes R., Becker A., Foreman-Mackey D., Deming D., 2016, *AJ*, **152**, 100  
Luger R., Lustig-Yaeger J., Agol E., 2017, *ApJ*, **851**, 94  
Luger R., Agol E., Foreman-Mackey D., Fleming D. P., Lustig-Yaeger J., Deitrick R., 2018a, preprint, [p. arXiv:1810.06559](https://arxiv.org/abs/1810.06559)  
(arXiv:1810.06559)

- Luger R., Kruse E., Foreman-Mackey D., Agol E., Saunders N., 2018b, *AJ*, **156**, 99
- Luque R., et al., 2019, arXiv e-prints, p. [arXiv:1904.12818](#)
- Malavolta L., et al., 2016, *A&A*, **588**, A118
- Malavolta L., et al., 2018, *AJ*, **155**, 107
- Meschiari S., Wolf A. S., Rivera E., Laughlin G., Vogt S., Butler P., 2009, *Publications of the Astronomical Society of the Pacific*, **121**, 1016
- Morton T. D., 2012, *ApJ*, **761**, 6
- Morton T. D., 2015, VESPA: False positive probabilities calculator, Astrophysics Source Code Library (ascl:1503.011)
- Nelson B. E., Ford E. B., Buchner J., Cloutier R., Díaz R. F., Faria J. P., Rajpaul V. M., Rukdee S., 2018, preprint, ([arXiv:1806.04683](#))
- Nutzman P., Charbonneau D., 2008, *PASP*, **120**, 317
- Parviainen H., 2015, *MNRAS*, **450**, 3233
- Pepe F., et al., 2004, *A&A*, **423**, 385
- Pepper J., Stassun K., Gaudi B. S., 2018, preprint, ([arXiv:1802.10158](#))
- Petigura E. A., et al., 2017, *AJ*, **153**, 142
- Pollacco D. L., et al., 2006, *PASP*, **118**, 1407
- Queloz D., et al., 2000, *A&A*, **354**, 99
- Rasmussen C. E., Williams C. K. I., 2006, *Gaussian Processes for Machine Learning*. MIT Press
- Reiners A., et al., 2018, *A&A*, **609**, L5
- Ribas I., et al., 2018, *Nature*, **563**, 365
- Ricker G. R., et al., 2015, *Journal of Astronomical Telescopes, Instruments, and Systems*, **1**, 014003
- Skilling J., 2004, in Fischer R., Preuss R., Toussaint U. V., eds, Vol. 735, *American Institute of Physics Conference Series*. pp 395–405, [doi:10.1063/1.1835238](#)
- Skilling J., 2009, in Goggans P. M., Chan C.-Y., eds, Vol. 1193, *American Institute of Physics Conference Series*. pp 277–291, [doi:10.1063/1.3275625](#)
- Sozzetti A., Torres G., Charbonneau D., Latham D. W., Holman M. J., Winn J. N., Laird J. B., O'Donovan F. T., 2007, *ApJ*, **664**, 1190
- Speagle J. S., 2019, arXiv e-prints, p. [arXiv:1904.02180](#)
- Stassun K. G., et al., 2018, *AJ*, **156**, 102
- Tak H., Ghosh S. K., Ellis J. A., 2018, *MNRAS*, **481**, 277
- Tinney C. G., Butler R. P., Marcy G. W., Jones H. R. A., Penny A. J., Vogt S. S., Apps K., Henry G. W., 2001, *ApJ*, **551**, 507
- Trotta R., 2008, *Contemporary Physics*, **49**, 71
- Tuomi M., Jones H. R. A., Barnes J. R., Anglada-Escudé G., Butler R. P., Kiraga M., Vogt S. S., 2018, *AJ*, **155**, 192
- Wheatley P. J., et al., 2013, in *European Physical Journal Web of Conferences*. p. 13002 ([arXiv:1302.6592](#)), [doi:10.1051/epjconf/20134713002](#)
- Winn J. N., 2010, preprint, ([arXiv:1001.2010](#))
- Wright J. T., Howard A. W., 2009, *ApJS*, **182**, 205
- Wright J. T., et al., 2011, *PASP*, **123**, 412
- Yi S., Demarque P., Kim Y.-C., Lee Y.-W., Ree C. H., Lejeune T., Barnes S., 2001, *ApJS*, **136**, 417

This paper has been typeset from a  $\text{\LaTeX}$  file prepared by the author.

**Table 10.** Posterior parameters obtained from our joint photometric and radial-velocity *juliet* analysis for the K2-32 multi-planet system.

Parameter name	Posterior estimate <sup>a</sup>
Posterior parameters for K2-32	
$\rho_*$	$2122.6^{+56.9}_{-62.3}$
Posterior parameters for K2-32b	
$P_b$	$8.991854^{+0.000089}_{-0.000093}$
$t_{0,b}$ (BJD UTC)	$2456909.91797^{+0.00031}_{-0.00028}$
$r_{1,b}$	$0.421^{+0.049}_{-0.051}$
$r_{2,b}$	$0.05496^{+0.00051}_{-0.00054}$
$K_b$ (m/s)	$5.63^{+0.78}_{-0.76}$
$e_b$	0 (fixed)
Posterior parameters for K2-32c	
$P_c$	$20.65974^{+0.00087}_{-0.00085}$
$t_{0,c}$ (BJD UTC)	$2456961.4058^{+0.0017}_{-0.0016}$
$r_{1,c}$	$0.538^{+0.032}_{-0.037}$
$r_{2,c}$	$0.03108^{+0.00054}_{-0.00056}$
$K_c$ (m/s)	$1.68^{+0.83}_{-0.82}$
$e_c$	0 (fixed)
Posterior parameters for K2-32d	
$P_d$	$31.7143^{+0.0013}_{-0.0011}$
$t_{0,d}$ (BJD UTC)	$2456903.7905^{+0.0016}_{-0.0018}$
$r_{1,d}$	$0.63156^{+0.02001}_{-0.02124}$
$r_{2,d}$	$0.03673^{+0.00059}_{-0.00064}$
$K_d$ (m/s)	$2.43^{+0.94}_{-0.87}$
$e_d$	0 (fixed)
Posterior parameters for K2 photometry	
$M_{K2}$ (ppm)	$-3500^{+860}_{-870}$
$\sigma_{w,K2}$ (ppm)	$83.6^{+1.1}_{-1.1}$
$q_{1,K2}$	$0.334^{+0.155}_{-0.104}$
$q_{2,K2}$	$0.61^{+0.19}_{-0.16}$
Posterior GP parameters for K2 photometry	
$\sigma_{\mathcal{GP},K2}$ (ppm)	$10.46^{+7.3}_{-4.3}$
$T_{K2}$ (days)	$16647^{+30333}_{-10917}$
$\rho_{K2}$ (days)	$49^{+24}_{-16}$
Posterior RV parameters	
$\mu_{\text{HIRES}}$ (m/s)	$-1.722^{+0.714}_{-0.705}$
$\sigma_{w,\text{HIRES}}$ (m/s)	$3.65^{+0.65}_{-0.56}$
$\mu_{\text{HARPS}}$ (m/s)	$1.092^{+0.701}_{-0.706}$
$\sigma_{w,\text{HARPS}}$ (m/s)	$3.92^{+0.67}_{-0.58}$
$\mu_{\text{PFS}}$ (m/s)	$-6.5^{+2.0}_{-2.0}$
$\sigma_{w,\text{PFS}}$ (m/s)	$4.6^{+2.2}_{-1.8}$

<sup>a</sup> Errorbars denote the 68% posterior credibility intervals.

**Table 11.** Derived parameters from our joint photometric and radial-velocity *juliet* analysis for the K2-32 multi-planet system.

Parameter name	Posterior estimate <sup>a</sup>
Derived parameters for K2-32b	
$R_{p,b}/R_*$	$0.05497^{+0.00052}_{-0.00054}$
$b_b = (a_b/R_*)\cos(i_{p,b})$	$0.135^{+0.074}_{-0.076}$
$(a_b/R_*)$	$20.85^{+0.18}_{-0.20}$
$i_{p,b}$ (deg)	$89.62^{+0.21}_{-0.21}$
Derived parameters for K2-32c	
$R_{p,c}/R_*$	$0.03108^{+0.00054}_{-0.00056}$
$b_c = (a_c/R_*)\cos(i_{p,c})$	$0.307^{+0.048}_{-0.056}$
$(a_c/R_*)$	$36.31^{+0.32}_{-0.35}$
$i_{p,c}$ (deg)	$89.51571^{+0.08934}_{-0.08008}$
Derived parameters for K2-32d	
$R_{p,d}/R_*$	$0.03673^{+0.00059}_{-0.00064}$
$b_d = (a_d/R_*)\cos(i_{p,d})$	$0.44734^{+0.03001}_{-0.03186}$
$(a_d/R_*)$	$48.32^{+0.42}_{-0.47}$
$i_{p,d}$ (deg)	$89.470^{+0.038}_{-0.038}$

<sup>a</sup> Errorbars denote the 68% posterior credibility intervals.